The Origin, Pathway, and Destination of Niño-3 Water Estimated by a Simulated Passive Tracer and Its Adjoint

ICHIRO FUKUMORI, TONG LEE, BENNY CHENG, AND DIMITRIS MENEMENLIS

Jet Propulsion Laboratory, California Institute of Technology, Pasadena, California

(Manuscript received 15 October 2002, in final form 12 May 2003)

ABSTRACT

The nature of subtropical–tropical water mass exchange in the Pacific Ocean is investigated, focusing on the origin, pathway, and destination of water occupying the surface layer of the eastern equatorial Pacific Ocean (Niño-3 region; 5°S–5°N, 150°–90°W). Simulated passive tracers and their adjoint are employed to explicitly follow the circulation of specific water masses accounting for advective and diffusive effects and their time variabilities. The evolution of the forward passive tracer and adjoint passive tracer can be identified as describing where the tracer-tagged water mass goes and from where it comes, respectively. Over 10 years on average, water mass of the Niño-3 region can be traced back to eastern subtropical thermocline waters of the Northern (27%) and Southern Hemispheres (39%). The Niño-3 water subsequently returns to these subtropical latitudes in the upper ocean. In contrast to the hypothesized ''subtropical cell,'' however, this circulation is an open circuit with water returning to the western regions of the two hemispheres (subtropical gyres) and to the Indian Ocean, instead of returning to its origins. The representative transit time scale from the subtropics to the Tropics is 10–15 yr. Temporal variability causes the tropical circulation inferred from a time-mean state to differ significantly from the average circulation. In particular, stirring due to nonseasonal, intra-annual variability significantly enhances the transport magnitude of the so-called interior pathways relative to that of the circuitous low-latitude western boundary pathways. Such short-circuit in the subtropical–tropical exchange may help better to explain tracer distributions, such as the observed midbasin tritium maximum in the equatorial Pacific Ocean. Significant differences in circulation pathways are also identified that are associated with El Niño and La Niña events. The strength of the subtropical–tropical water mass exchange is estimated to have weakened during the 1990s.

1. Introduction

The persistent warming of the tropical Pacific Ocean during 1992–94 (e.g., Ji et al. 1996) has stimulated investigations into low-frequency changes of the tropical ocean—in particular, that of El Niño [or El Niño–Southern Oscillation (ENSO)]. Subtropical–tropical water mass exchange has been identified as part of a possible mechanism by which the mean state of the tropical Pacific Ocean may be slowly altered, resulting in decadal variability in the period and strength of ENSO. Noting that the time scale of advection from the subtropics to the Tropics is comparable to that of the observed changes of ENSO, Gu and Philander (1997) postulate that thermal anomalies subducted in the subtropics, its subsequent advection to the Tropics, and its interaction with the atmosphere may explain such interdecadal changes observed in the tropical Pacific Ocean.

Indeed Deser et al. (1996) identified a cold anomaly in the central North Pacific Ocean (~35°N) subducting in the late 1970s from the surface down into the main thermocline that subsequently propagated toward lower latitudes (~25°N) over a decade. Zhang et al. (1998) observed similar warm anomalies in the subtropical gyre originating in the early 1970s that subducted and penetrated toward the Tropics circulating clockwise around the subtropical gyre. However, the fate of such anomalies, in particular, whether the anomalies actually reach the equator, is somewhat unclear. For instance, Schneider et al. (1999) suggest that observed temperature anomalies have different characteristics between locations north and south of 18°N; changes equatorward of 18°N are observed to be driven mostly by local wind stress curl rather than propagating thermal anomalies from the subtropics. (See also Nonaka et al. 2002.)

Compelling evidence of water of subtropical origin reaching the equator is provided by the distribution of tritium, a passive tracer of mainly anthropogenic origin generated by atmospheric testing of nuclear weapons in the Northern Hemisphere in the early 1960s. Tritium distribution within the thermocline of the Pacific Ocean shows a distinct tongue of high values extending southwestward from the eastern subtropics toward the Tropics (Fine et al. 1981). Tritium distribution along the equator is nonzero, indicating contribution of water of northern

Corresponding author address: Dr. Ichiro Fukumori, Jet Propulsion Laboratory, Mail Stop 300-323, California Institute of Technology, 4800 Oak Grove Drive, Pasadena, CA 91109-8099.
E-mail: fukumori@jpl.nasa.gov

origin. In particular, tritium concentration along the equator is maximum in the central Pacific (Fine et al. 1987).

The so-called subtropical cell (STC; McCreary and Lu 1994) provides a theoretical description of the subtropical–tropical water mass exchange. The STC consists of water mass subducting in the subtropics, equatorward flow in the thermocline, upwelling at the equator, and poleward return flow in the surface layer that closes the circulation. The equatorward component of the thermocline flow is bounded on the east by the shadow zone of the ventilated thermocline and to the west by the recirculating region of the subtropical gyre (McCreary and Lu 1994; Liu 1994).

The pathway by which the subtropical waters reach the Tropics has been the subject of several studies, motivated in part by the observed tritium distribution described above. The equatorward flow of the STC can be separated into water that directly reaches the equator in the interior of the ocean and water that flows via the low-latitude western boundary currents (LLWBCs; Liu et al. 1994). Simple depth-integrated transport calculations based on wind estimates imply geostrophic flow converging toward the equator in the central Pacific (McPhaden and Fine 1988; Huang and Wang 2001). Whereas the direct interior pathway to the equator appears to be present in the Southern Hemisphere, most numerical simulations suggest that the equatorward transport in the interior of the North Pacific is limited, as reflected by the high potential vorticity area under the intertropical convergence zone (ITCZ; Liu and Huang 1998; Lu et al. 1998).

Based on hydrographic observations, Johnson and McPhaden (1999) estimate the magnitude of the interior equatorward mass transport in the thermocline of the Pacific Ocean to be 5 and 15 Sv (Sv $\equiv 10^6$ m^3 s^{-1}) in the Northern and Southern Hemispheres, respectively. The discrepancy between the two hemispheres reflects the presence of the aforementioned high potential vorticity ''barrier'' in the North Pacific. In comparison, Butt and Lindstrom (1994) estimate the magnitude of the LLWBC mass transports reaching the equator to be 13 and 12 Sv for the Mindanao Current and the New Guinea Coastal Undercurrent, respectively.

Ocean general circulation models provide comparable estimates to the observed time-mean circulation (Rothstein et al. 1998; Huang and Liu 1999). Moreover, simulations by Coles and Rienecker (2001) suggest a possible seasonal modulation of the interior mass exchange, with largest equatorward flow occurring during the autumn and early winter. Effects of the time-variable circulation on the subtropical–tropical mass exchange remain one of the leading uncertainties in existing studies. For instance, fluxes associated with tropical eddy activity is comparable to surface forcing and may contribute to the nature of this exchange (Lu and McCreary 1995).

The present study examines the subtropical–tropical mass exchange in the Pacific Ocean using a realistic simulation of the time-varying circulation. Effects of mixing and time variability are taken into consideration, in addition to time-mean advection, by quantifying the exchange using a simulated passive tracer and its adjoint. As described in section 2, integration of the passive tracer and its adjoint can be interpreted, respectively, as describing where the tracer-tagged water mass goes and where the water comes from. This study focuses on the water mass occupying the Niño-3 area, the surface layer in the eastern equatorial Pacific Ocean between 5°S and 5°N and between 150° and 90°W. Sea surface temperature in Niño-3 provides one of the key indices of ENSO. Understanding the origin and pathway of the water mass occupying this area could help shed light onto the nature of El Niño and its variability.

In section 2, we describe the model used in this study. Aspects of this model's circulation are examined in relation to other studies in section 3. In section 4, we discuss the physical significance of passive tracers and their adjoint. Then in section 5, these passive tracers are used to examine the origin, pathway, and destination of the Niño-3 water mass; the exchange pathways are identified and their strengths are quantified. The effect of intraseasonal variability is examined by comparisons with solutions based on time-mean circulations. We conclude with a summary and discussion in section 6.

2. Model description

The model employed in this study is based on a parallel version of the Massachusetts Institute of Technology (MIT) general circulation model (Marshall et al. 1997). The model domain is nearly global, extending from 80°S to 80°N, with a fairly high spatial resolution designed to better simulate the seasonal to interannual changes of the upper ocean circulation. Horizontal grid spacing is 1° globally, except within 20° of the equator, in which meridional grid spacing is gradually reduced to 0.3° within 10° of the equator. Vertical grid spacing is 10 m within 150 m of the surface, gradually increasing to 400 m toward the bottom of the domain. The total number of grid points is 360 by 224 by 46, zonally, meridionally, and vertically, respectively.

The vertical mixing scheme of Large et al. (1994) is employed for realistic simulation of near-surface mixing processes. Convection is achieved by dramatically increasing the vertical mixing coefficient (from 5×10^{-6} to 0.1 m^2 s^{-1}) wherever the stratification is statically unstable. Computationally, vertical diffusion is implemented by an implicit time-stepping scheme. Mixing effects of mesoscale eddies are represented using the Redi (1982) isoneutral mixing scheme and the Gent and McWilliams (GM) parameterization (Gent and McWilliams 1990). The GM–Redi coefficient is tapered as per Large et al. (1997).

The model is initially at rest with climatological temperature and salinity distributions (Levitus et al. 1998). The model is spun up for 10 years, forced by time-mean

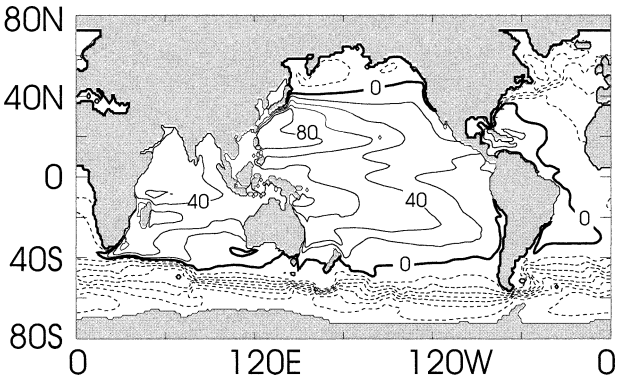

FIG. 1. Time-mean model sea surface height averaged from 1980 to 2000. Sea level is measured with respect to its global mean. Contour interval is 20 cm. The thick curve is 0 cm. Negative (positive) values are shown in dashed (solid) contours.

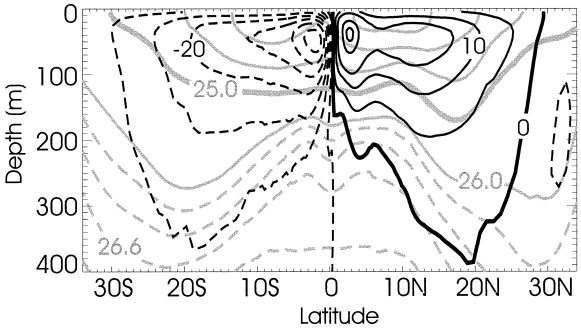

FIG. 2. Time-mean (1980–2000) meridional overturning streamfunction in the Pacific Ocean (black contours and labels). Contour interval is 5 Sv. Negative (positive) values are shown in dashed (solid) contours. The thick curve is 0 Sv. Gray contours and gray labels are the time-mean, zonally integrated, potential density (σ_θ). Contour intervals of density are 1 and 0.2 kg m^{-3} for solid and dashed contours, respectively. Thick solid gray contour is 25 kg m^{-3}. Meridional transport south of the Indonesian passage, defined by the region west of the northern tip of New Guinea (0.3°N), is corrected for the Indonesian Throughflow (13 Sv) by assuming this return flow occurs uniformly in depth. (Meridional transport in the South Pacific is otherwise not closed and a meridional overturning streamfunction cannot be defined.)

seasonal wind stress and heat flux climatologies (da Silva et al. 1994). Following the spinup, the model is forced from 1980 to 2001 by wind stress, heat flux, and evaporation minus precipitation estimates of the National Centers for Environmental Prediction (NCEP)–National Center for Atmospheric Research (NCAR) Reanalysis Project (Kalnay et al. 1996). (Results described in this study are not sensitive to the particular spinup above. For instance, experiments based on another simulation from 1980 to 2001, but one using the end state of 2001 above as initial condition, yields similar results.) Sea surface temperature is further relaxed to observed temperatures (Reynolds and Smith 1994) with a spatially varying relaxation coefficient computed from the NCEP–NCAR product using the method employed by Barnier et al. (1995). The equivalent of a fresh water flux is implemented by relaxing surface salinity to climatological values with a 60-day relaxation coefficient. To correct for the somewhat weaker equatorial winds of the NCEP–NCAR reanalysis in comparison with other estimates (e.g., satellite scatterometer measurements and climatology of da Silva et al. 1994), a spatially varying but time-invariant correction is applied to the reanalysis estimates. This wind correction is defined as the mean difference between the climatological estimates and corresponding NCEP–NCAR reanalysis between 1993 and 1997; that is, the time-mean winds of the NCEP–NCAR reanalysis are replaced by those of da Silva et al. (1994).

3. Model time-mean circulation

Aspects of the model's simulated circulation are illustrated in Figs. 1, 2, and 3. Figure 1 shows the model's time-mean sea level, averaged from 1980 to 2000, illustrating the model domain and the spatial variability of mean sea level associated with the major surface currents across the globe. The model has an open Indonesian passage with time-mean net transport of 13 Sv flowing from the North Pacific to the Indian Ocean (Lee et al. 2002).

The model's time-mean, zonally integrated, meridional overturning streamfunction of the tropical Pacific Ocean shows the structure and extent of the subtropical cell (McCreary and Lu 1994) near the surface (Fig. 2). Poleward flow in the surface layer is compensated by strong upwelling along the equator that is fed by equatorward flow in the thermocline. Downwelling from the surface into the thermocline occurs over a wide latitudinal extent off the equator up to about 30° latitude. In addition to the broad STC, the so-called tropical cell (TC; Lu et al. 1998) is also evident in Fig. 2. As compared with the STC, the depth range of the TC is much shallower and its meridional extent is much smaller. The TC is confined roughly to within 5° of the equator and to depths above 100 m. The distinction between the STC and TC is more obvious in the Northern Hemisphere where the combined meridional circulation cell shows two separate centers about 50-m depth, one at about 3°N and another at 12°N. The net strength of the shallow meridional overturning circulation is 31 and 38 Sv in the Northern and Southern Hemispheres, respectively.

The structure of the model's thermocline (pycnocline) in the Pacific Ocean is illustrated by the $\sigma_\theta = 25$ kg m^{-3} surface in Fig. 3. The depth of this isopycnal (Fig. 3a) reflects the deepening of the thermocline toward the west along the equator. The east–west undulation of the contours immediately north of the equator corresponds to the alternating zonal equatorial current system (South Equatorial Current, North Equatorial Countercurrent, and North Equatorial Current). The $\sigma_\theta = 25$ kg m^{-3} surface is deepest toward the western North Pacific at about 16°N. The large meridional gradient north of this

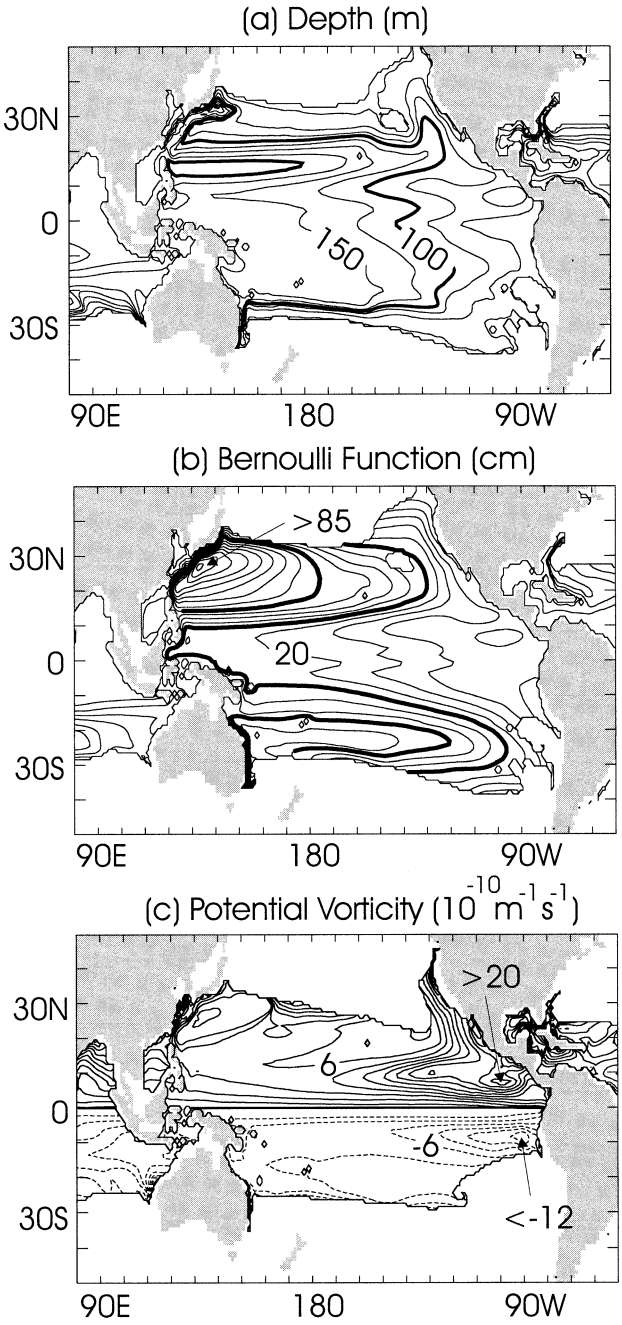

FIG. 3. The 1980–2000 time-mean $\sigma_\theta = 25$ kg m^{-3} surface: (a) depth (m), (b) Bernoulli function (in equivalent sea level, cm; $B\rho_o^{-1}g^{-1}$), and (c) planetary potential vorticity (10^{-10} m^{-1} s^{-1}). Contour intervals are (a) 25 m, (b) 5 cm, and (c) 2×10^{-10} m^{-1} s^{-1}. Potential vorticity is computed between $\sigma_\theta = 24.5$ and 25.5 kg m^{-3}. Negative values are shown as dashed contours. Thick curves in (b) denote contours bounding the subtropical gyres in the Northern (45 cm) and Southern (40 cm) Hemispheres and the equatorward flow via the LLWBCs (25 cm). Thick curve in (c) is zero potential vorticity (equator).

minimum (~20°N) corresponds to the subtropical countercurrent (e.g., Qiu 1999). Also evident is the large gradient associated with the Kuroshio south of Japan. This density surface outcrops at about 30°S and 35°N in each hemisphere, on average, with the outcrop in the eastern domain occurring farther north than that at the western end for both hemispheres.

Horizontal circulation on this isopycnal is illustrated in Fig. 3b by the Bernoulli function B (Rothstein et al. 1998):

$$B(\sigma) = \rho_o g\eta + g\int_{z(\sigma)}^{0} [\rho - \rho(\sigma)]\, dz, \qquad (1)$$

where σ in (1) is the density of the particular layer of interest, the 25 kg m^{-3} surface for Fig. 3b; ρ_0 is surface density, g is gravitational acceleration, η is sea level, and z is depth. The Bernoulli function can be identified as geostrophic streamlines away from the equator with flow parallel to B in the direction with high values on the right (left) facing downstream in the Northern (Southern) Hemisphere. Figure 3b illustrates the flow within the subtropical gyres bounded by $B\rho_o^{-1}g^{-1} = 45$ and 40 cm in the Northern and Southern Hemispheres, respectively. The equatorward flow via the LLWBCs occurs approximately between these boundaries and $B\rho_o^{-1}g^{-1} = 25$ cm, with the interior pathway outlined by smaller values of $B\rho_o^{-1}g^{-1}$. (These bounding values are indicated by thick contour lines in Fig. 3b). The time-mean net southward mass (volume) transport in the thermocline ($\sigma_\theta = 23$~26.5 kg m^{-3}) in the western boundary current and in the interior at 8.4°N (latitude where model Mindanao Current transport is largest between $\sigma = 23$ and 26.2 kg m^{-3}) is 9 and 5 Sv, respectively. In comparison, the corresponding net northward transport at 5.7°S is 11 and 9 Sv.

The planetary component of potential vorticity on the isopycnal $\sigma_\theta = 25$ kg m^{-3} (Fig. 3c) illustrates the high potential vorticity ridge in the North Pacific under the ITCZ extending westward from the eastern end of the basin. A similar anomaly (valley) exists in the Southern Hemisphere but with a smaller magnitude and a smaller spatial extent. The interior circulation, as inferred by the Bernoulli function (Fig. 3b), flows around these potential vorticity anomalies as the flow approaches the equator.

The circulation described in Figs. 1, 2, and 3 is comparable to results of observations and other modeling studies (e.g., Levitus 1982; Johnson and McPhaden 1999; Talley 1988; Rothstein et al. 1998) and illustrates that the general circulation simulated by the model is sensible and realistic.

4. Passive tracer and its adjoint

Passive tracers evolve according to advection and mixing of the water mass such that, in the absence of sources and sinks, changes in tracer distribution can be

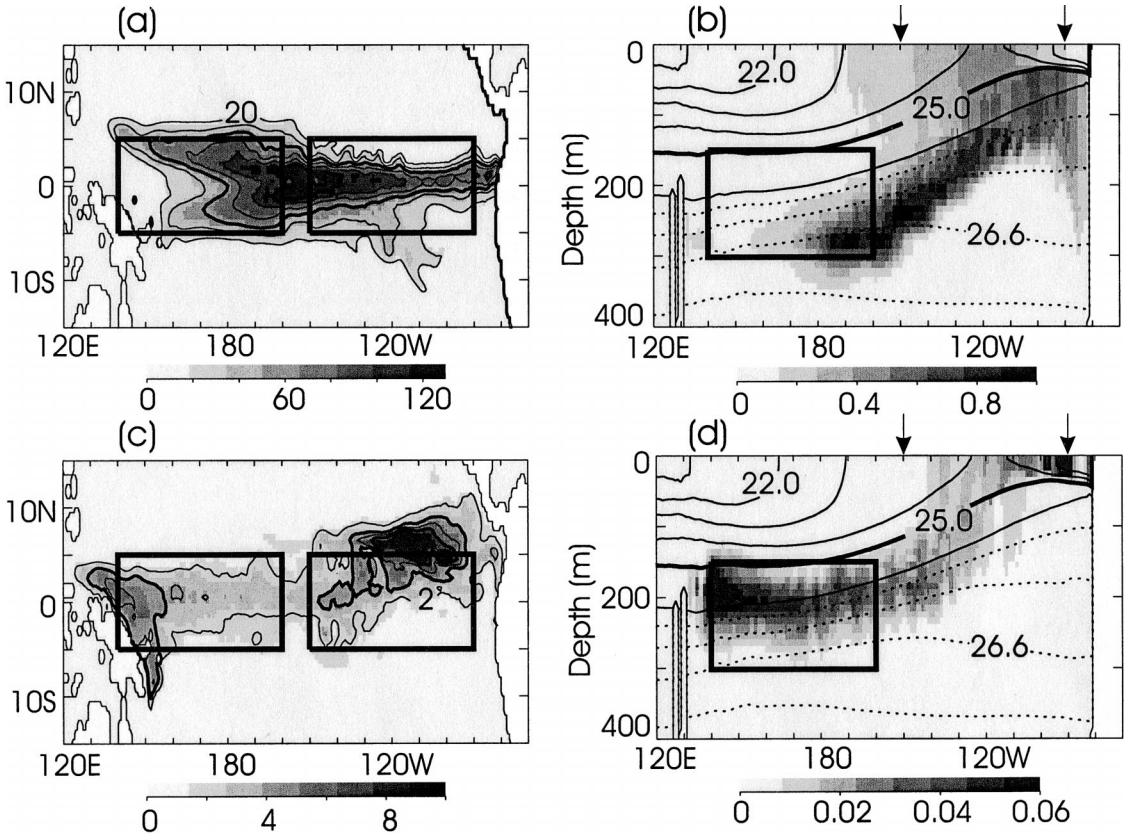

FIG. 4. An example of tracer and adjoint tracer distribution: (a) vertical integral and (b) zonal section of tracer and (c) vertical integral and (d) zonal section of adjoint tracer. Tracers are in arbitrary tracer units (ATU): ATU m^{-2} for (a) and (c) and ATU m^{-3} for (b) and (d). The outlined boxes correspond to areas of initial tracer and adjoint tracer release. See text for details. Contour intervals in (a) and (c) are 20 and 2 ATU m^{-2}, respectively. Contours in (b) and (d) are time-mean potential density; contour intervals are 1 kg m^{-3} (solid) and 0.2 kg m^{-3} (dashed). The thick contour in (b) and (d) is $\sigma_\theta = 25$ kg m^{-3}. Arrows in (b) and (d) indicate zonal boundaries of Niño-3.

used to identify origins and pathways of the tracer-tagged water mass and thus the circulation. Tritium has been employed to infer the direct connection between water in the equatorial ocean and water subducted in the subtropics (Fine et al. 1981, 1987). Coles and Rienecker (2001) employed a simulated passive tracer in their numerical circulation model to identify subducting pathways of thermocline water.

In the context of a general circulation model, the temporal evolution of a passive tracer is dictated by the same advection–diffusion equation as temperature and salinity, except for possible tracer sources and sinks, and differences in external forcing and boundary condition:

$$\frac{\partial c}{\partial t} = -\mathbf{u} \cdot \nabla c + \nabla \cdot \kappa \nabla c. \qquad (2)$$

Here c is the tracer concentration, $\mathbf{u}$ is the three-dimensional velocity vector, and κ is the mixing tensor. Sources and sinks of the tracer as well as fluxes through boundaries are assumed to be absent. Convection and various advanced mixing schemes (Gent and McWilliams 1990; Large et al. 1994) can be formulated into three-dimensional tensors in the form of (2). Effects of double diffusion are also implicitly incorporated into the mixing tensor.

An example of tracing the circulation of a particular water mass is shown in Fig. 4. Figures 4a and 4b show an evolution of a passive tracer patch after one year of integrating (2) using time-varying model velocity and mixing fields averaged every 10 days. [Considerable computational simplifications can be achieved by approximating (2) using such precomputed circulation fields. See the appendix for details.] The tracer was initialized uniformly to a unit value (in arbitrary tracer units per volume, ATU m^{-3}) on 1 January 2000 between 150- and 300-m depth, 5°S and 5°N, and 140°E and 160°W. After one year, the concentration of the tracer of this initial patch evolves because of advection and mixing; The water mass (tracer) along the equator has extended eastward (Fig. 4a) because of the Equatorial Undercurrent that gradually rises toward the surface in the eastern equatorial Pacific (Fig. 4b). The water mass upwells and mixes vertically across isopycnals outcrop-

ping in the eastern domain (Fig. 4b). Near the surface, the water mass spreads poleward because of Ekman transport and is advected westward along the equator by the South Equatorial Current. The tracer concentration values have decreased from their initial state because of mixing and stirring effects of the inhomogeneous velocity field, although the total tracer content is conserved (no sources or sinks).

Given the initial condition (1 ATU m^{-3} at the origin) and the fact that the tracer evolves identically with the water mass within the model, the tracer values can be interpreted as the fraction of water originating from the initial tracer-tagged water mass. For instance, a value of 0.3 ATU m^{-3} at the surface at 0°N, 100°W in Fig. 4b indicates that 30% of the water mass at this location originated from the initial patch and that the rest (70%) was advected and/or mixed in from somewhere else to this location.

Passive tracers are useful in describing the circulation and mixing of water forward in time. Specifically, the passive tracer evolution describes where the water mass goes. However, tracers do not readily describe from where the water came. In the example above, although 30% of the water is identified to have come from the initial patch, 70% came from elsewhere. To resolve from where this other 70% came, one would have to repeat the tracer release experiment from other possible locations, repeating until all water is accounted for. Analysis of this water's origin at different times would require separate integrations from different initial conditions (i.e., different initial times).

Equation (2) cannot be integrated backward in time in the presence of finite mixing. Mathematically, (2) cannot strictly be inverted because the equation is rank deficient, and therefore numerical integration of (2) backward in time is unstable. Physically, (2) cannot be integrated backward in time because of degeneracy due to mixing; once mixed there is no telling how to uniquely partition (''unmix'') specific elements of a water mass.

Tracing a given water mass backward in time can be achieved unambiguously within the context of the model simulation by a single integration of the adjoint of the passive tracer equation. Vukićević and Hess (2000) describe such interpretation of the adjoint tracer in the continuous framework. Here we demonstrate the physical significance of the passive tracer adjoint in finite difference form.

The physical significance of the passive tracer adjoint can be identified by considering dependencies of the passive tracer content for the particular volume defining the subject water mass to tracer concentrations in the past. Past tracer concentrations can affect the subject tracer content only if the past water mass or a part of it is advected or mixed into the target volume. This sensitivity, which can be identified as the adjoint of a passive tracer, thus quantifies past distribution of the given water mass.

Consider an objective function J in discretized form defined by the tracer content at time step t at a particular spatial grid point i:

$$J = \mathbf{e}_i^{\mathrm{T}}\mathbf{c}(t). \tag{3}$$

Here $\mathbf{c}(t)$ is a column vector of tracer concentration at all model grid points at time t. Vector $\mathbf{e}_i$ is a vector of zeroes except at the particular grid point of interest (i) where the element is 1. [Bold lower- (upper) case letters will denote column vectors (matrices), respectively.] Using the chain rule, the sensitivity of J with respect to tracer concentrations at time step $t - N$ ($t - N \le t$) can be written as

$$\frac{\partial J}{\partial \mathbf{c}(t-N)} = \frac{\partial \mathbf{c}(t-N+1)^{\mathrm{T}}}{\partial \mathbf{c}(t-N)} \frac{\partial \mathbf{c}(t-N+2)^{\mathrm{T}}}{\partial \mathbf{c}(t-N+1)} \cdots \frac{\partial \mathbf{c}(t)^{\mathrm{T}}}{\partial \mathbf{c}(t-1)} \frac{\partial J}{\partial \mathbf{c}(t)}. \tag{4}$$

By definition (3), the last term in (4) is simply

$$\frac{\partial J}{\partial \mathbf{c}(t)} = \mathbf{e}_i. \tag{5}$$

The tracer evolution, (2), is a homogeneous equation (no sources or sinks) and is linear with respect to tracer distribution, and can be written in finite-difference form as

$$\mathbf{c}(t) = \mathbf{A}(t-1)\mathbf{c}(t-1), \tag{6}$$

where $\mathbf{A}$ is the model's state transition matrix (Jacobian matrix). [Second-and-higher-order time-stepping schemes can be written in the form of (6), but with $\mathbf{c}$ consisting of tracers at multiple time-steps concatenated into a single column vector.] Then,

$$\frac{\partial \mathbf{c}(t)^{\mathrm{T}}}{\partial \mathbf{c}(t-1)} = \mathbf{A}^{\mathrm{T}}(t-1), \tag{7}$$

defining the finite-difference form of the tracer equation's adjoint. Using (5) and (7), (4) can be written as

$$\frac{\partial J}{\partial \mathbf{c}(t-N)} = \mathbf{A}^{\mathrm{T}}(t-N)\mathbf{A}^{\mathrm{T}}(t-N+1) \cdots \mathbf{A}^{\mathrm{T}}(t-1)\mathbf{e}_i. \tag{8}$$

Multiplying from right to left, (8) shows that the sensitivity of the tracer at location i at time t (the objective function, J) to the tracer distribution at time $t - N$ [$\mathbf{c}(t - N)$] is given by integrating the adjoint tracer equation ($\mathbf{A}^{\mathrm{T}}$) backward in time from t to $t - N$ with terminal condition $\mathbf{e}_i$ at time t. As discussed above, this sensitivity can be identified as describing where the water mass defined by J was at time $t - N$. Given the terminal condition of unity at the target grid point i ($\mathbf{e}_i$), the resulting value of the adjoint tracer at each grid point corresponds to the fraction of that water mass that makes its way to point i at time t. The water distribution at earlier times can be evaluated by extending the adjoint

integration (8) further back in time, without starting the evaluation anew.

Given the linearity of the tracer evolution equation (and its adjoint) with respect to its concentration, the source of the water mass over a finite region can be deduced by integrating the adjoint equation with an initial condition, **e**, that is zero everywhere except within the volume of interest where it is uniformly 1. For example, Figs. 4c and 4d show the distribution of an adjoint tracer patch integrated backward in time for 1 year from 31 December 2000 that was initialized to a uniform value in the top 10 m in Niño-3 (5°S–5°N, 150°–90°W). [The resulting adjoint tracer evolution is an example of a ''boundary propagator'' of Holzer and Hall (2000) that is related to a Green's function.] Distribution of this adjoint tracer indicates that part of the water in Niño-3 was in the thermocline in the western equatorial Pacific 1-yr prior, reflecting the eastward advection by the Equatorial Undercurrent and subsequent upwelling. The adjoint tracer concentration in January 2000, like the tracer values in Figs. 4a and 4b, is smaller than its terminal value on 31 December 2000 because of mixing and stirring effects before reaching Niño-3.

Comparison of the tracer and its adjoint shows consistency between the two inferences of the circulation. In the example above, the average tracer content in the surface layer of Niño-3 on 31 December 2000 is 0.256 ATU m^{-3}. Namely, 25.6% of the water mass in Niño-3 on 31 December 2000 originated from the thermocline box (box where tracer was released with unit concentration) in the western equatorial Pacific on 1 January 2000. Consistent with this estimate, the total adjoint tracer content in this western equatorial thermocline box on 1 January 2000 is 25.6% of the total initial adjoint tracer released in Niño-3 on 31 December 2000. The exact correspondence between these two estimates demonstrates the consistency between physical interpretations of the evolution of a passive tracer and that of its adjoint; that is, the two describe where the tracer-tagged water mass goes and where the adjoint tracer tagged water mass comes from, respectively. Their value, when initialized to unity, describe the fractional content at each location of the original tracer- and adjoint tracer-tagged water mass.

The two tracer solutions contain complementary information. While both tracers can be used to deduce how much water from the western box reaches Niño-3, they also describe where the rest of the water goes and from where the rest of the water comes, respectively—information that is not immediately available by the other.

Note again that one is not the inversion of the other, or vice versa [cf. (2), above, and (A1) in the appendix]. For instance, in the presence of mixing, running the adjoint tracer equation backward in time from a particular tracer distribution does not recover the initial forward tracer distribution. This is because, once mixed, elements of the mixed water mass are no longer distinguishable from one another and thus a tracer evolution is noninvertable. However, mixing coefficients define rates at which water is mixed and thus an unambiguous deduction is possible of what fractions of the water mass originated from where (equivalent to adjoint tracer) even though identification of particular water particles (forward tracer) is not possible. Adjoint passive tracers define the fraction of the water mass as opposed to identifying any particular water particle.

Considerable computational simplification is achieved by approximating (2) using precomputed circulation fields. Implementation of the adjoint tracer model can also be simplified by employing the same numerical code for the forward tracer model but reversing the sign of the time derivative (i.e., integration backward in time) and that of the circulation (i.e., eastward velocity changed to westward velocity of same magnitude, etc.). See the appendix for further discussion. Differences with solutions without these approximations are minor and therefore analyses below will employ these simplifications.

5. Pathway of Niño-3 Water

Sources and pathways of water mass in the surface layer of the Niño-3 region are examined using the general circulation model described in section 2. An adjoint passive tracer and a forward passive tracer are utilized in turn by tagging this water mass (''Niño-3 water'') to study from where the water comes and where it goes, respectively.

a. From where does Niño-3 water come?

To examine time-dependencies of the circulation and to establish a mean climatological pathway, adjoint tracer integrations were conducted and compared starting from different instances (different terminal times). In each experiment, an adjoint passive tracer is initialized to a unit value in the surface layer (10 m thick) of Niño-3 at a particular instant (''Niño-3 initialization'') and is integrated backward in time. Figure 5 compares the depth-integrated adjoint tracer content of five of such experiments after integrating backward for 5 years. Each panel in Fig. 5 corresponds to starting the integration from different terminal times; from the end of 1999 (Fig. 5a) to the end of 2000 (Fig. 5e). Apart from differences towards the eastern end of the basin (labeled A in Fig. 5c), differences largely occur on interannual time scales (e.g., difference between Figs. 5a and 5e being larger than between Figs. 5a and 5c), such as the magnitude of the tracer near LLWBCs (B and C in Figs. 5a and 5e, respectively) and the meridional extent of the tracer distribution (labeled D in Fig. 5b). As described below, Niño-3 water in the eastern end of the basin (A) accounts for a small fraction of the total Niño-3 water and is part of a near-surface pathway that is distinct from the dominant thermocline pathways of STC. Further analyses

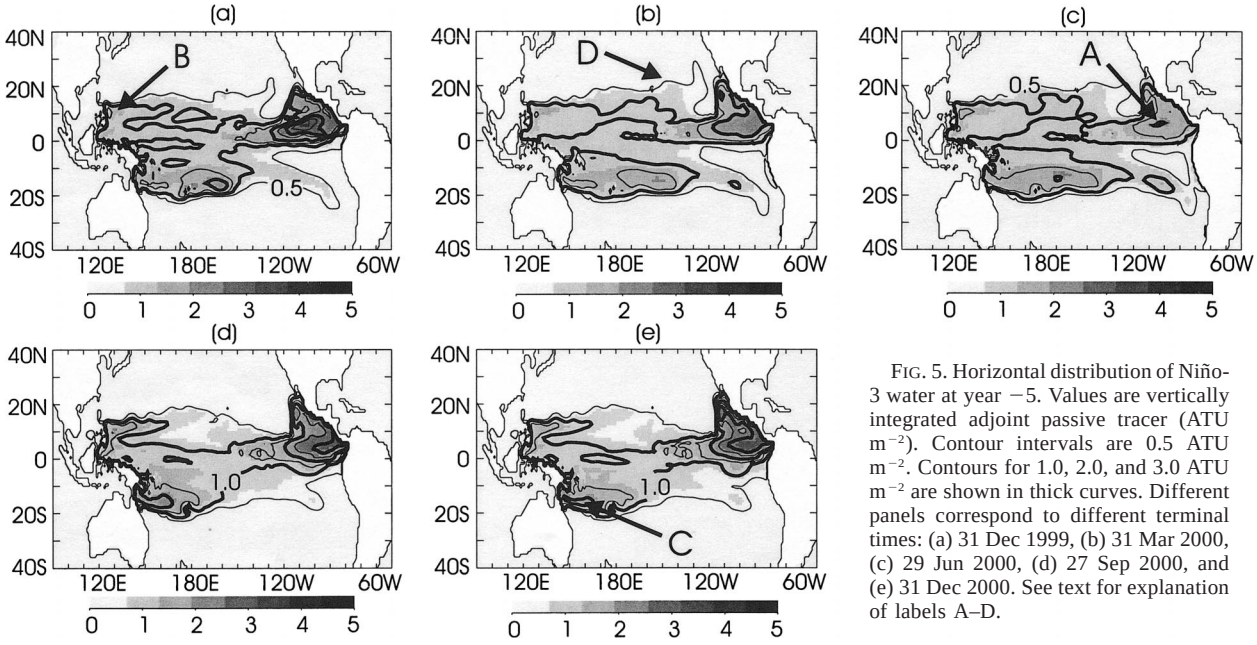

FIG. 5. Horizontal distribution of Niño-3 water at year −5. Values are vertically integrated adjoint passive tracer (ATU m^{-2}). Contour intervals are 0.5 ATU m^{-2}. Contours for 1.0, 2.0, and 3.0 ATU m^{-2} are shown in thick curves. Different panels correspond to different terminal times: (a) 31 Dec 1999, (b) 31 Mar 2000, (c) 29 Jun 2000, (d) 27 Sep 2000, and (e) 31 Dec 2000. See text for explanation of labels A–D.

will therefore focus on the circulation's interannual dependency unless noted otherwise.

A mean climatological pathway of the Niño-3 water circulation is estimated by averaging adjoint tracer distributions of different experiments. The experiments consist of 10 backward 10-year-long, adjoint tracer integrations, each starting from the end of different years from 1991 to 2000. An average adjoint tracer distribution is then computed by averaging these 10 results according to relative time from the respective terminal instant. (See section 5d for a discussion on interannual differences among these experiments.) Figure 6 shows the average depth-integrated adjoint tracer distribution as a function of years from the terminal time.

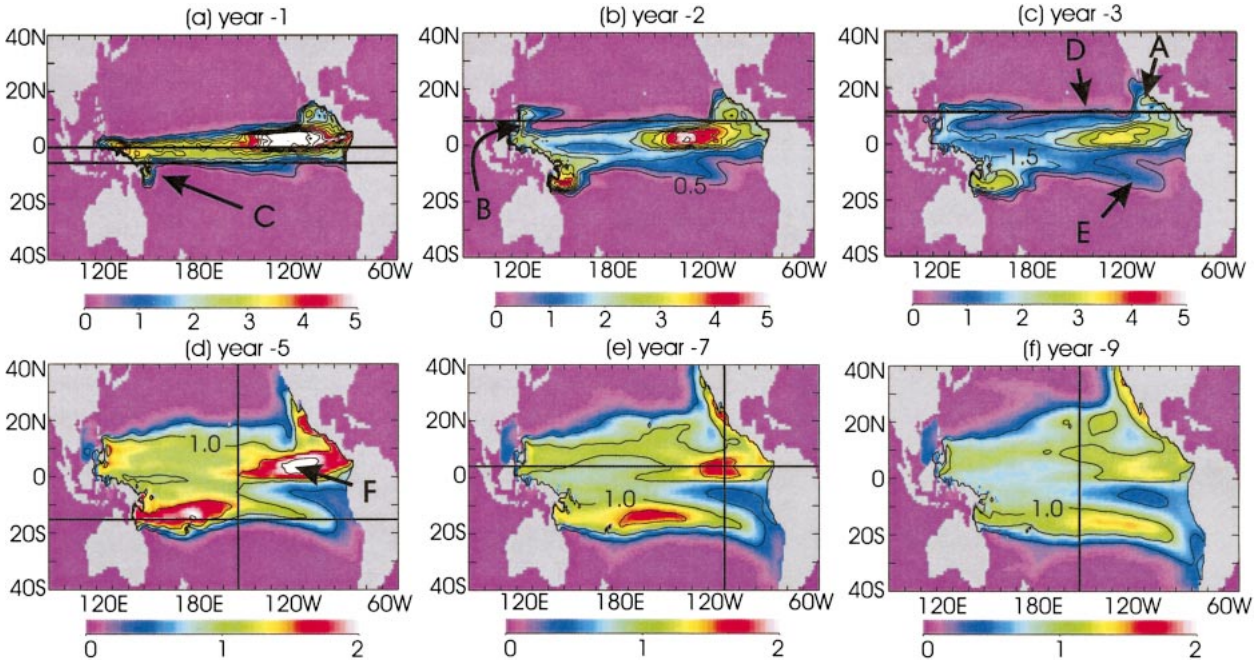

FIG. 6. Average horizontal distribution of Niño-3 water as a function of years from terminal time in reverse chronological order: years (a) −1, (b) −2, (c) −3, (d) −5, (e) −7, and (f) −9. Values are adjoint passive tracer integrated vertically (ATU m^{-2}). Distribution at terminal instant (year 0) is uniformly 10 (ATU m^{-2}) within Niño-3 and zero elsewhere. Contour intervals are 0.5 ATU m^{-2}, and are shown from 0.5 to 6.0 ATU m^{-2}. Solid lines indicate location of vertical sections shown in Fig. 7.

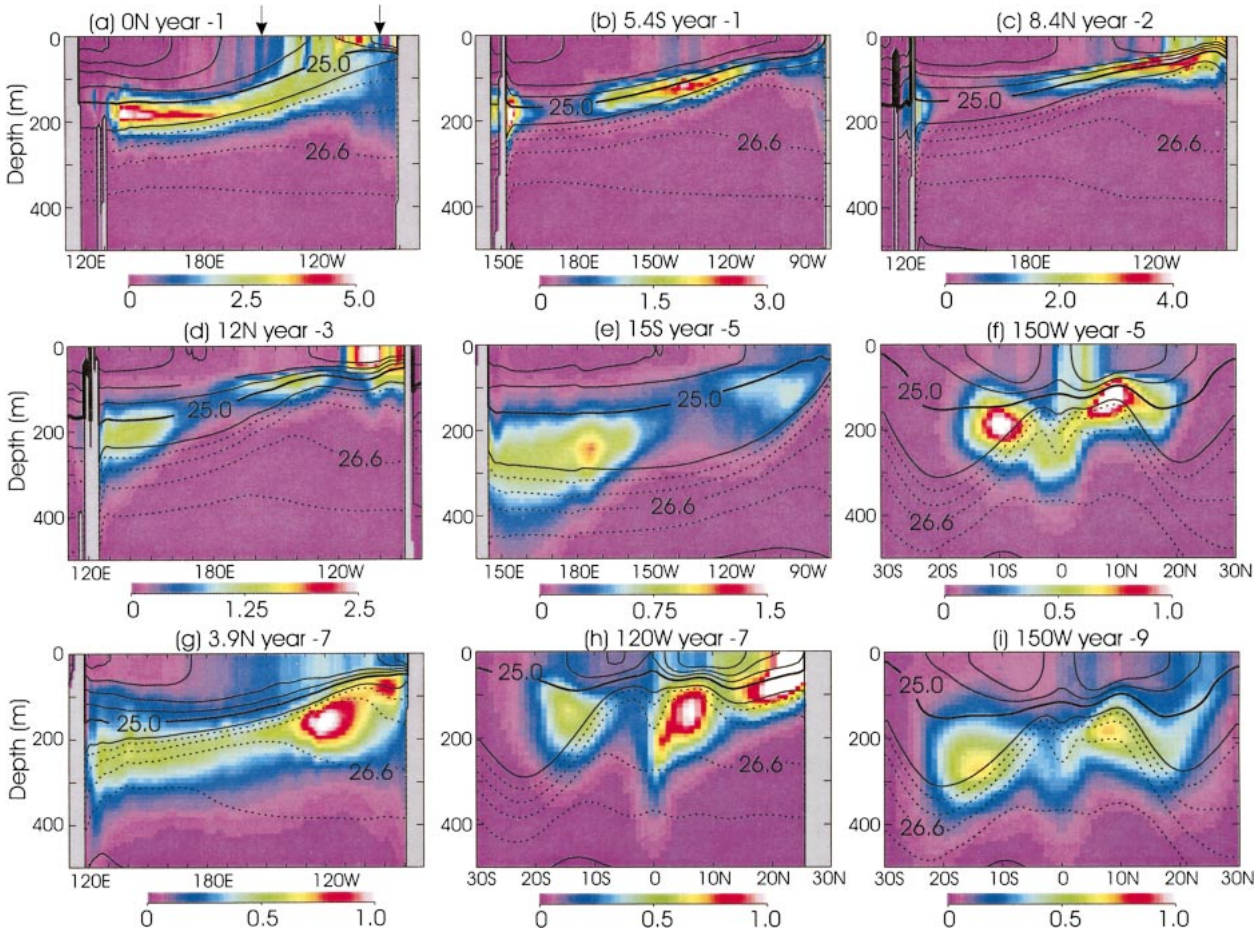

FIG. 7. Vertical cross sections of average Niño-3 water distribution along select latitudes and longitudes at different times from the terminal instant in reverse chronological order: (a) 0°N year −1, (b) 5.4°S year −1, (c) 8.4°N year −2, (d) 12°N year −3, (e) 15°S year −5, (f) 150°W year −5, (g) 3.9°N year −7, (h) 120°W year −7, and (i) 150°W year −9. Units are 10^{-2} ATU m^{-3}. Potential density surfaces are indicated by contours; solid contours are at intervals of 1 kg m^{-3}. Thick solid curve is $\sigma_\theta = 25$ kg m^{-3}. Dashed contours are at intervals of 0.2 kg m^{-3}, and are shown for isopycnals larger than 26 kg m^{-3}. Arrows in (a) indicate boundaries of Niño-3.

The depth integrated time series (Fig. 6) illustrate the lateral circulation of the Niño-3 water mass before reaching Niño-3 at year 0. Water from the eastern subtropics gradually flow equatorward (Figs. 6f–d), whereupon the water rapidly converges zonally toward Niño-3 within a few years (Figs. 6c–a). In the interior, westward flow of the equatorward circulation is evidenced in Figs. 6f to 6d by the westward movement of the high-concentration area in the Southern Hemisphere and the gradual western intensification (adjoint tracer convergence) in the Northern Hemisphere east of the Philippines.

The horizontal circulation indicates several distinct sources and pathways of the Niño-3 water. These include water originating from the coastal regions of North and Central America (indicated as A in Fig. 6c) and fluxes along the western boundary in the Northern (B in Fig. 6b) and Southern Hemispheres (C in Fig. 6a). Interior pathways are also evident in both hemispheres as indicated by symbols (in Fig. 6c) D and E in the Northern and Southern Hemispheres, respectively. Note the gradual equatorward convergence of the tonguelike feature corresponding to E from Fig. 6f to Fig. 6a. The corresponding feature in the Northern Hemisphere is less obvious but can be identified by the broad tonguelike feature of the contour corresponding to 0.5 ATU m^{-2} (Figs. 6a–c). A ''pool'' of high Niño-3 water content (F in Fig. 6d) is present through most of the 10-yr period in the northern part of Niño-3 and the region immediately to its north (approximately 0°–8°N, 130°–90°W). This pool, in turn, is fed by water from the interior (D) and coastal pathways (A) and gradually moves westward with time (cf. Figs. 6e and 6b). Hardly any water originates from the Indian Ocean because, on average, the water flows from the Pacific Ocean to the Indian Ocean.

Vertical cross sections of the mean adjoint tracer evolution are shown in Fig. 7 along select sections in space and time indicated by solid lines in Fig. 6. By and large, the pathway of Niño-3 water is found within the ther-

mocline. In terms of volume, 70% of the Niño-3 water is found below 50 m between density surfaces 23 and 26.5 kg m^{-3}, 5 years prior to reaching Niño-3.

Along the equator at year −1, Niño-3 water is found largely toward the western end of the equatorial thermocline (Fig. 7a). Regions with high adjoint tracer concentration along this section correspond to the depth of the Equatorial Undercurrent that carries this water mass eastward and upward toward Niño-3, where the water mixes vertically and upwells to the surface one year later. Off the equator (Figs. 7b,c), at latitudes near the core of the low-latitude western boundary currents, the adjoint tracer distribution shows distinct zonal separation between water in the LLWBC and the interior. At earlier times, and farther upstream away from the equator, water feeding the LLWBCs is found extending away from the western boundary (Figs. 7d,e). The adjoint tracer at 15°S (Fig. 7e) is found over a larger depth range than at 5.4°S (Fig. 7b) corresponding to a broader thermocline in depth. In the Northern Hemisphere (Fig. 7d), three distinct patches are evident, corresponding to water feeding the LLWBC (Mindanao Current) pathway in the west and the interior pathway in the central Pacific, both within the thermocline, and water at the eastern end found at the surface. The last patch corresponds to water in the coastal pathway along North and Central America identified as A in Fig. 6c. Most of the water in the ''Niño-3 pool'' (F in Fig. 6) is found below the pycnocline (Figs. 7g,h) southwest of the Costa Rica Dome, indicated by the doming of the thermocline about 100°W (e.g., Fiedler 2002). Meridional sections along 150°W (Figs. 7f,i) illustrate the meridional pathway of the adjoint tracer conforming to undulations of the thermocline. The latitudinal extent of the adjoint tracer patch found in the thermocline moves equatorward from year −9 (Fig. 7i) to year −5 (Fig. 7f). The Niño-3 water also gradually upwells with time as evidenced by the adjoint tracer distribution moving toward lighter density surfaces. Outcropping of the Niño-3 water in the subtropics is evident about 20°–30°N at year −9 (Fig. 7i). These subtropical outcroppings will be revisited below.

The adjoint tracer's horizontal extent is largely coincident with the time-mean circulation within the thermocline, consistent with the tracer's depth distribution. Figure 8 shows the mean meridional transport streamfunction within the thermocline between σ_θ = 23 and σ_θ = 26.2 kg m^{-3} overlaid on top of the maximum value of the depth-integrated tracer content over 10 years at each location. The western boundary source region coincides with the LLWBCs. In particular, the northern extent of the adjoint tracer east of the Philippines matches the boundary between stream functions feeding the Kuroshio to the north and the Mindanao Current to the south. In the Southern Hemisphere, the mushroom-shaped cloud of adjoint tracer southeast of New Guinea (Fig. 6b) agrees with the source region of the model's equivalent of the New Guinea Coastal Undercurrent. Unlike the Northern Hemisphere, stream functions of the thermocline defining the Southern Hemisphere subtropical gyre are mostly connected to the LLWBC, and consequently the adjoint tracer invades the center of the gyre in the Southern Hemisphere but not in the Northern Hemisphere. The eastern extent of the adjoint tracer distribution away from the equator also largely coincides with the thermocline circulation, except for the water mass along the coast of Central and North America, which occupies the surface (Fig. 7d).

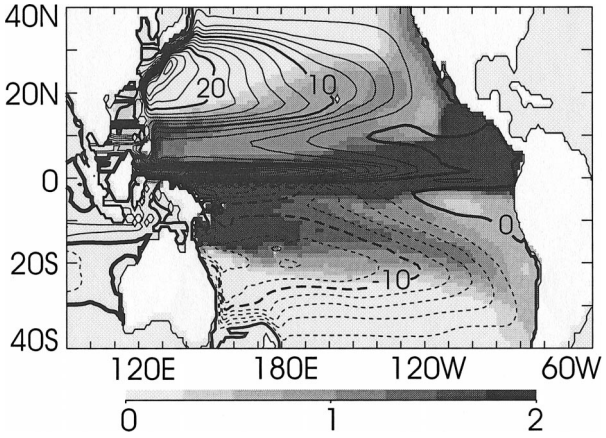

FIG. 8. Transport streamfunction within the thermocline (contours) below 50-m depth between σ_θ = 23 and 26.2 kg m^{-3}. Contour interval is 2 Sv. Negative (positive) values are shown in dashed (solid) contours. Also shown in shades of gray is the maximum depth integrated average adjoint tracer content over 10 years (ATU m^{-2}) illustrating the pathway of the Niño-3 water.

The relative strengths of the LLWBC and the interior pathways are examined by computing their respective meridional transport. Figure 9 shows zonal sections of net meridional advective transport of the adjoint tracer over 10 years along 5.7°S and 8.4°N, corresponding to latitudes of maximum meridional transport of the LLWBCs of the respective hemispheres (Fig. 8). The corresponding diffusive flux is an order of magnitude smaller than the advective component along these sections. Distinct patches of transport can be identified, corresponding to the various sources indicated in Fig. 6. The adjoint tracer transport within the LLWBCs are of the highest transport per unit area of these sections and are found to extend to depths and density surfaces deeper than the thermocline. The LLWBC transports are also accompanied by opposite transports within recirculation zones offshore. Most of the interior transport occurs within the thermocline east of 180° at both latitudes. Wind-driven Ekman transport at the surface carries the adjoint tracer in opposite directions above the interior thermocline transport and corresponds to the upper branch of the STC (Fig. 2). The shallow meridional pathway off Central America is evidenced by the southward flux at the surface about 110°W in Fig. 9b. This southward flux is accompanied by a northward flux also at the surface to its east, that reflects recirculation

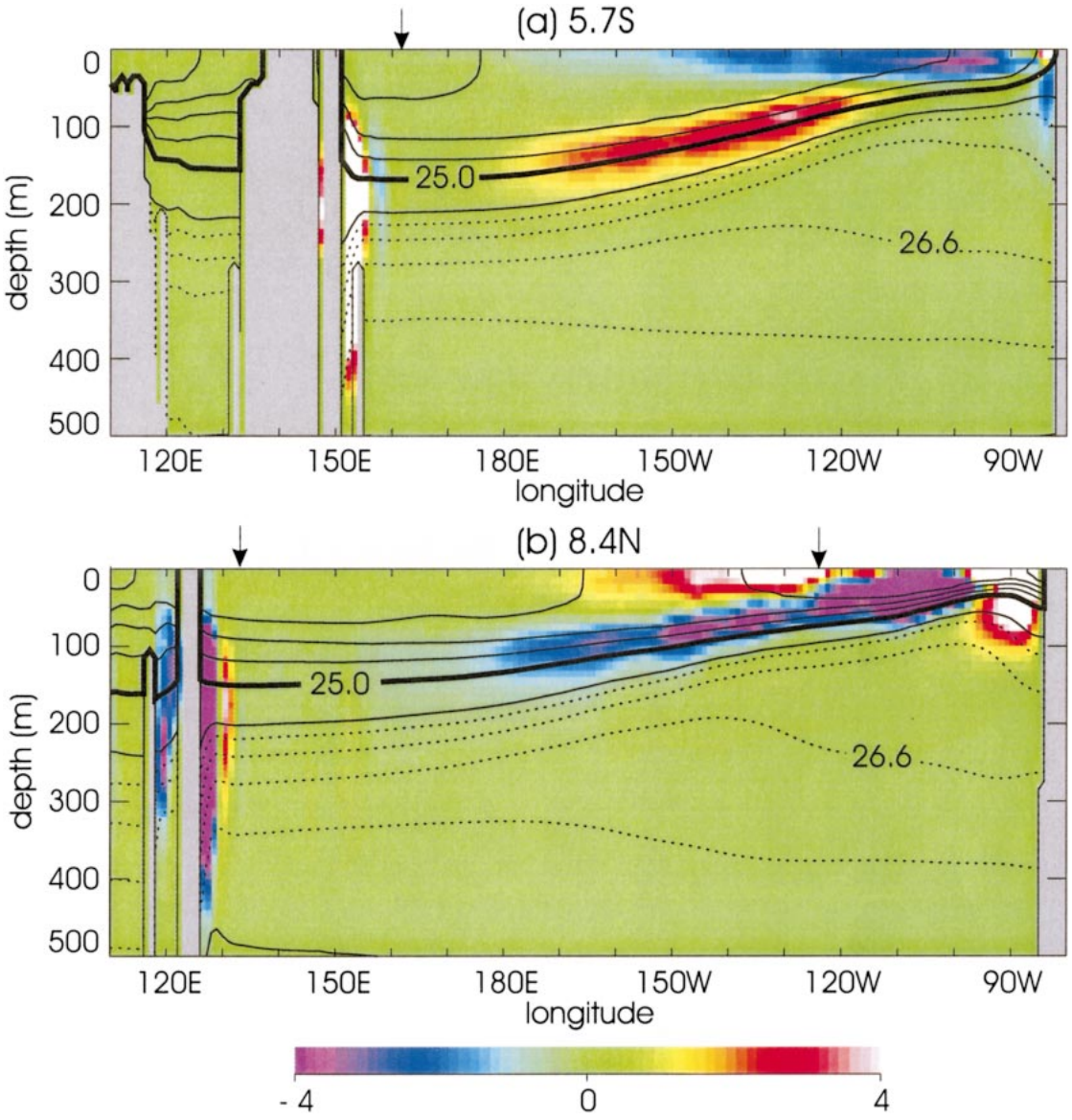

FIG. 9. Average net meridional advective transport of adjoint tracer over 10 years; (a) 5.7°S and (b) 8.4°N. Northward flux forward in time is shown positive. Contours are time-mean potential density, as in Fig. 7. Arrows at top indicate boundaries used in delineating transport in Table 1 for the low-latitude western boundary current (162°E at 5.7°S and 133°E at 8.4°N) and the Costa Rica Dome region (124°W at 8.4°N). Units are 10^4 ATU m^{-2}.

associated with the Costa Rica Dome, evidenced by the doming of the thermocline.

The net meridional flux of the respective pathways was computed by integrating the flux vertically from the surface to the bottom and zonally between longitudes indicated by the arrows at the top of Fig. 9. The Ekman transport contribution during the first 10 years of adjoint tracer integration arises largely from local vertical transport of Niño-3 adjoint tracer south of the thermocline outcrop region, as opposed to water that circuits the STC. (See transit time scale in the following section.) Thus the corresponding source (transport) of this Ekman flux in the thermocline water does not reflect a net meridional transport of Niño-3 water and is removed by the surface-to-bottom integration. The net meridional flux is tabulated in Table 1. LLWBCs are defined by regions west of 162°E at 5.7°S and west of 133°E at 8.4°N. These LLWBC boundaries are determined as longitudes east of the western boundary recirculation regions where net meridional transports change sign. The Costa Rica Dome region (CRD) is defined by longitudes east of 124°W at 8.4°N and is determined as the longitude where the depth-integrated adjoint tracer is locally minimum at year −5 (similar at other instances).

Of the water that will make up Niño-3 water in 10

TABLE 1. Net adjoint tracer transport over 10 years across 5.7°S and 8.4°N for different experiments: average among the 10 experiments with different terminal years (''average''), time-mean circulation (''steady''), and mean annual cycle (''seasonal''). Northward transport with time is shown as positive. LLWBCs are defined by regions west of 162°E at 5.7°S and west of 133°E at 8.4°N. The CRD is defined by longitudes east of 124°W at 8.4°N. (Delineations are indicated by arrows in Fig. 9.) Units are 10^{12} in the arbitrary tracer unit (ATU). Percentages given in parentheses are those of each total transport, whereas those in brackets for the total are percentages of the net adjoint tracer over the entire ocean. The total adjoint tracer content is 76.8×10^{12} ATU.

Lat	Expt	Total	LLWBC	Interior	CRD
5.7°S	Average	29.8 [39%]	23.0 (77%)	6.8 (23%)	
	Steady	33.3 [43%]	28.0 (84%)	5.3 (16%)	
	Seasonal	31.4 [41%]	27.1 (86%)	4.3 (14%)	
8.4°N	Average	−24.5 [32%]	−15.8 (64%)	−4.8 (20%)	−3.9 (16%)
	Steady	−17.6 [23%]	−17.3 (98%)	−0.1 (1%)	−0.2 (1%)
	Seasonal	−21.8 [28%]	−19.5 (90%)	−1.6 (7%)	−0.7 (3%)

years, on average, 32% and 39% originate from the extratropics north and south of the equator, respectively, as defined by latitudes of maximum LLWBC thermocline transport (8.4°N and 5.7°S). Of the extratropic transport in the Southern Hemisphere, 77% and 23% flow through the LLWBC and interior pathways, respectively. The extratropic transport in the Northern Hemisphere is composed of 64% LLWBC flux, 20% interior transport, and 16% flux near the eastern boundary.

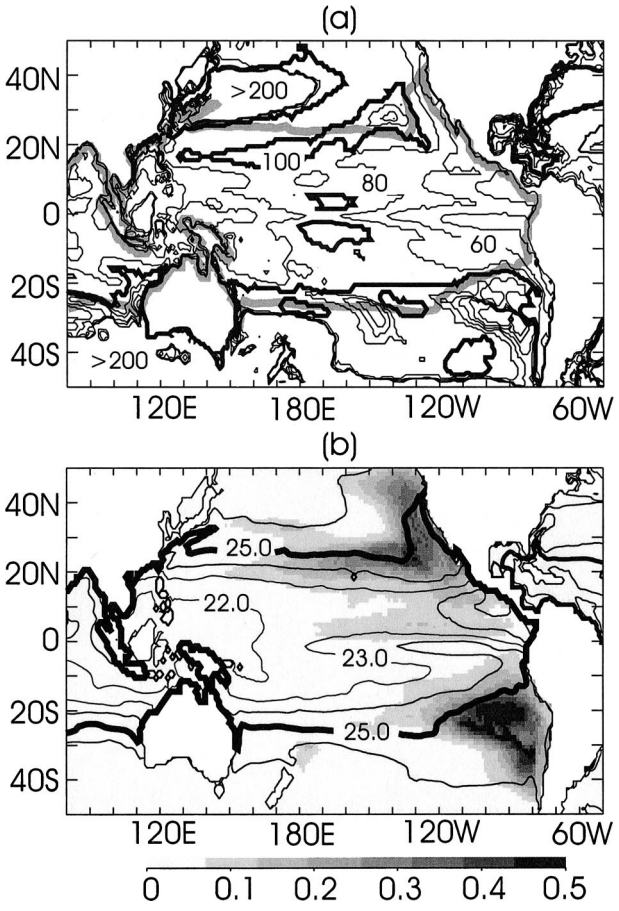

FIG. 10. (a) Mixed layer depth (m) and (b) the average adjoint tracer content within the mixed layer at year −10 (ATU m^{-2}). Contours in (b) are maximum surface density of the average annual cycle. Contour intervals are 20 m and 1 kg m^{-3}, and the thick solid curves correspond to 100 m and 25 kg m^{-3}, in (a) and (b), respectively. The gray curve in (a) is the 25 kg m^{-3} curve in (b). The mixed layer is defined by the maximum depth at which density is within 0.125 kg m^{-3} of that of the surface.

Some of the thermocline transport can be traced back to the surface, as evidenced by outcroppings of the adjoint tracer in Fig. 7i. Water in contact with the atmosphere at the beginning of year −10 (10 years prior to reaching Niño-3) is shown in Fig. 10, defined by integrated adjoint tracer content within the surface mixed layer. Here, the mixed layer is defined by the maximum depth at which density is within 0.125 kg m^{-3} of that of the surface (Levitus 1982). Nearly equal amounts of adjoint tracer are found in the Northern (≥8.4°N) and Southern (≤5.7°S) Hemisphere mixed layers, each amounting to approximately 8% of the initial total Niño-3 water content. Figure 10b also illustrates that the outcropped water in the Northern Hemisphere is slightly lighter than those in the Southern Hemisphere, as evidenced by the location of the $\sigma = 25$ kg m^{-3} contour with respect to the adjoint tracer distribution. Such difference is also evident in the adjoint tracer distribution within the interior thermocline pathway (cf. Figs. 7b and 7c and Figs. 7d and 7e). Additionally, outcropping in the Southern Hemisphere is confined more to the eastern end of the basin in comparison with the outcroppings in the Northern Hemisphere.

b. Transit time

The adjoint tracer evolution (Fig. 6) indicates water mass at midlatitudes requiring nearly 10 years to reach the Tropics. Because water of any given volume can take multiple pathways to the target region, transit times can only be discussed within an average statistical framework. Moreover, mean transit times, defined as the first moment of the transit time probability density function (pdf), are sensitive to the tail of the pdf and are not necessarily a representative time scale (Holzer and Hall 2000). Here we define representative transit times as the time at which the maximum adjoint tracer concentration is attained (i.e., the statistical mode of transit time distribution). For instance, Fig.

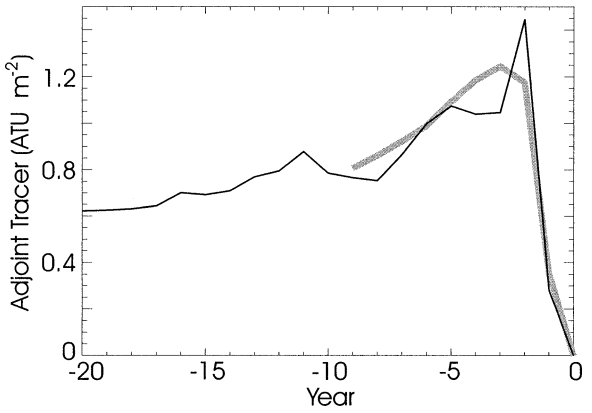

FIG. 11. Time series of depth-integrated adjoint tracer content (ATU m^{-2}) at 11°N, 156°E. The gray curve is the average tracer content among the 10 experiments ending between 1991 and 2000. The solid curve corresponds to a 20-yr adjoint tracer integration from the end of 2000 to 1981.

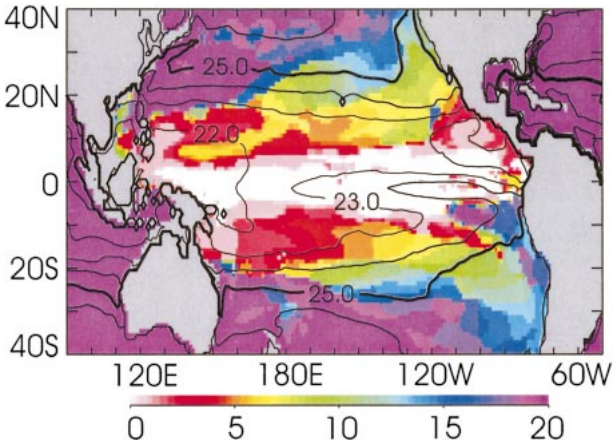

FIG. 12. Depth-averaged representative transit time (yr) to Niño-3, based on a 20-yr backward integration of the Niño-3 adjoint tracer from the end of 2000. Transit time is defined as the statistical mode of a transit time probability density function. Contours are of surface density as in Fig. 10b.

11 shows time series of depth integrated tracer content at 11°N, 156°E. The representative transit time for this location is 3 years as indicated by the time when the gray curve attains its maximum value. Because representative transit times of Niño-3 water at midlatitudes are approximately 10 years, the 10-yr integration employed in estimating the average circulation is not sufficiently long to avoid ambiguities. Instead, transit times here will be estimated based on a particular 20-yr adjoint tracer integration starting from the end of 2000. Time series of the depth integrated adjoint tracer content at 11°N, 156°E for this particular experiment are comparable with the average evolution, as shown by the black curve in Fig. 11.

The spatial dependence of representative transit times based on the particular 20-yr integration is shown in Fig. 12. The pattern is consonant with the average tracer evolution shown in Fig. 6. Transit times are less than 1 year along the equator, but increase rapidly away from the equator reaching 10–15 years in the subduction zones in the eastern subtropical basin (Fig. 10). Tongue-like structures are evident in the transit time distribution that correspond to the mean pathways identified in Fig. 6. Representative transit times from the core of the LLWBCs are 1 year or less. The Northern Hemisphere interior pathway has a slightly longer transit time scale than that in the Southern Hemisphere at comparable latitudes away from the equator.

c. Effects of time-varying circulation

Although intra-annual differences in the source and pathway of Niño-3 water are relatively small (Fig. 5), the underlying variability in the circulation can nevertheless be fundamental in mixing and stirring and thus important in defining the pathway of a given water mass. To assess the impact of the circulation's intra-annual variability, pathways associated with the time-mean circulation are derived and compared with the average pathway of the time-variable circulation discussed above (''average''; Fig. 6). Two time-mean circulations are considered by averaging the velocity and mixing coefficients over the 20-yr period of interest from 1981 to 2000. A time-invariant circulation (''steady'') is defined by averaging over the entire 20-yr period, and a mean annual cycle (''seasonal'') is computed by averaging the circulation as a function of day-of-the-year over the 20-yr period.

Figure 13 compares the depth integrated adjoint tracer content after 5 years of backward integration using these two circulation fields in comparison with the average adjoint tracer distribution discussed above (Fig. 6). Notable differences are found in the relative strengths of the different sources and pathways identified in the previous section.

The coastal source along North America present in the average time-variable circulation (Fig. 13a) is absent in both of the time-mean circulations (Figs. 13b,c). This absence is primarily due to differences in mixing as shown in Fig. 14. Figure 14 compares adjoint tracer content near the surface (50 m) after a one-year integration when either advection or mixing is replaced by its respective mean annual cycle. Also shown for comparisons are results for the mean annual circulation (seasonal) (Fig. 14d) and the time-variable circulation integrated from the end of 2000 (Fig. 14a). Results with average mixing have the least adjoint tracer content near the surface. Because the near-surface circulation drives the Costa Rica Dome intrusion of the adjoint tracer (Figs. 7d and 9b), the lesser surface adjoint tracer content results in a smaller intrusion along the coast. The larger effective mixing associated with the mean mixing coefficients can be ascribed to artificial cross isopycnal

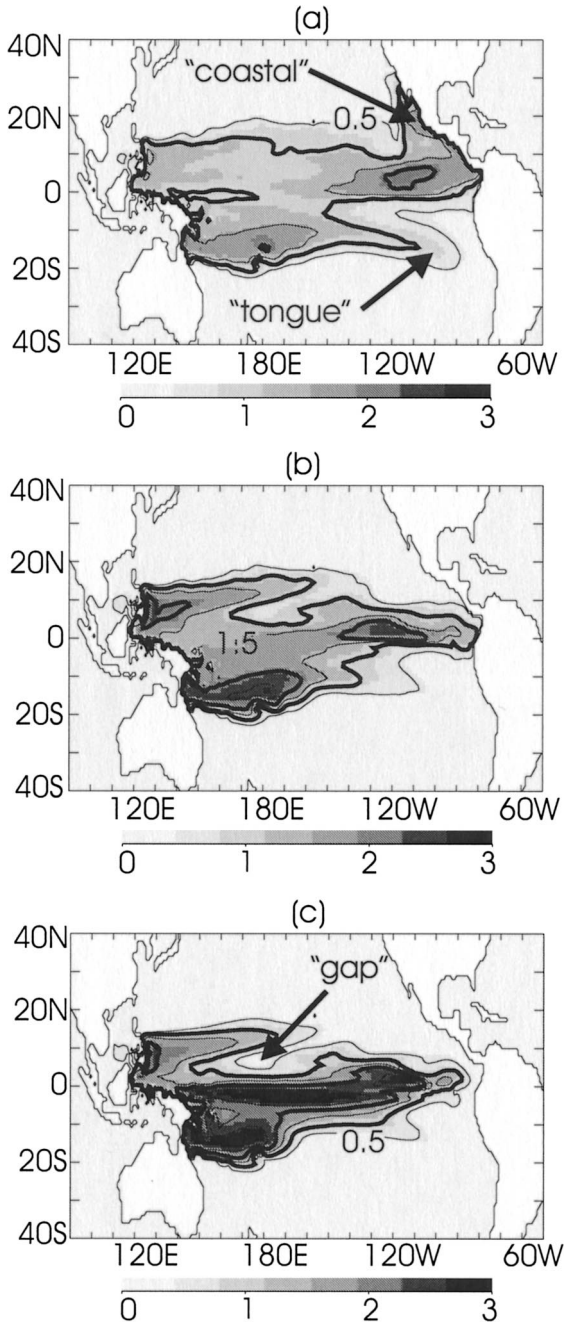

FIG. 13. Horizontal distribution of Niño-3 water at year −5 using different circulation estimates: (a) average distribution as in Fig. 6 (average), (b) mean seasonal cycle (seasonal), and (c) time-invariant mean circulation (steady). Values are vertically integrated adjoint passive tracer (ATU m^{-2}). Contours are as in Fig. 5; Contour intervals are 0.5 ATU m^{-2} and values for 1.0, 2.0, and 3.0 ATU m^{-2} are shown in thick contours. Pathway of Niño-3 water depends significantly on the circulation's time variability. See text for details.

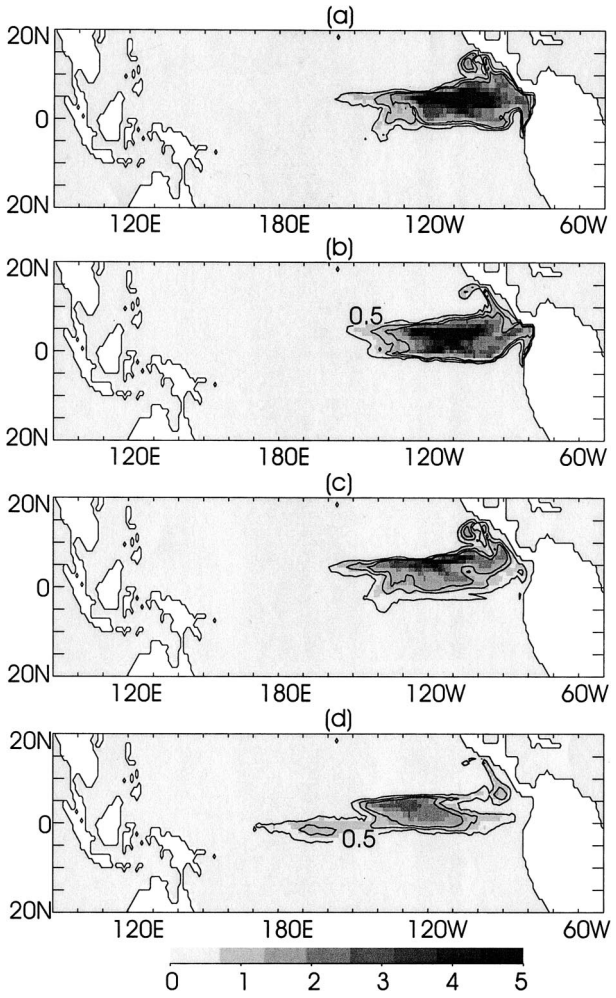

FIG. 14. Adjoint tracer content (ATU m^{-2}) in the top 50 m at year −1. Different panels compare effects of filtering the circulation field (velocity and mixing) in time: (a) unfiltered time-variable circulation, (b) mean annual cycle velocity and time-variable mixing, (c) time-variable velocity and mean annual cycle mixing, and (d) mean annual cycle circulation (seasonal). The spatially integrated adjoint tracer content for each of these results in the top 50 m is (a) 22.2×10^{12} ATU (29% of the total tracer content), (b) 20.3×10^{12} ATU (26%), (c) 14.9×10^{12} ATU (19%), and (d) 12.0×10^{12} ATU (16%). Time-variable circulation is based on year 2000. Contours are shown for 0.5, 1.0, and 1.5 ATU m^{-2}.

mixing due to time averaging of mixing in depth coordinates.

Other differences in Fig. 13 include features due to an apparent weakness in the interior pathway for the two time-mean circulations. For instance, a ''gap'' (denoted in Fig. 13c) is present in the adjoint tracer content between the LLWBC and interior pathways in the Northern Hemisphere for the seasonal (Fig. 13b) and steady (Fig. 13c) circulation. Similarly, the latitudinal extent of the tonguelike structure of the southern interior pathway is shorter in the steady circulation (Figure 13c) than in the average circulation (Fig. 13a).

The net meridional transport of the Niño-3 adjoint tracer corresponding to these experiments is computed as in other experiments, and its values are tabulated at 5.7°S and 8.4°N in Table 1 for comparison. The LLWBC

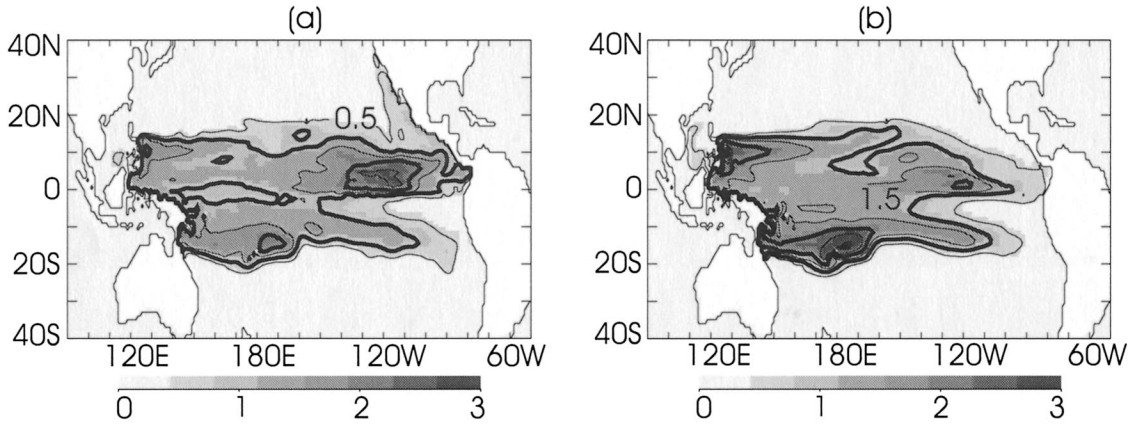

FIG. 15. (a) Horizontal distribution of 1994 Niño-3 water at year −5 (end of 1989) and (b) its equivalent using a low-pass-filtered circulation. Values are vertically integrated adjoint passive tracer (ATU m^{-2}). Contours are as in Figs. 5 and 13; Contour intervals are 0.5 ATU m^{-2} and values for 1.0, 2.0, and 3.0 ATU m^{-2} are shown in thick contours. Adjoint tracers are integrated from the end of 1994. The low-pass filtering is defined as a 1-yr running average.

transport of the Niño-3 adjoint tracer for the time-mean circulation (steady) is relatively larger than that of the interior pathway in comparison with those of the average circulation (average) in both hemispheres. The weaker interior pathways can be attributed to the absence of temporal variations in the circulation. The time-variable circulation acts as an agitator straining and stirring water parcels, transporting parts of it, and making them subject to different parts of the general circulation that carry them elsewhere, similar to stirring cream poured in coffee or tea.

To assess the relative effect of the circulation's intra-annual and interannual variability, the adjoint tracer evolution for the 10-day running mean circulation (default model resolution; see section 4) is compared with that using a 1-yr running mean (Fig. 15). The water mass distributions of the two circulations (Figs. 15a and 15b) are similar to those of the average among circulations (Fig. 13a) and the mean seasonal cycle (Fig. 13b), respectively. The net interior transport over 10 years for the two experiments is 25% and 14% (20% and 14%) of the net southward (northward) transport at 8.4°N (5.7°S), respectively. Differences in the relative magnitude of the interior pathways are similar to those between results of the average and seasonal circulation (Table 1). Thus the difference among the water mass distribution in Fig. 13 is mostly due to the circulation's intra-annual variability as opposed to interannual differences. (See the next section for discussion on interannual differences.)

The significance of the circulation's temporal variability in defining pathways of water masses warrants further consideration. In particular, the equatorial domain is a region with one of the largest temporal variabilities on the globe. These variabilities include equatorial waves, instability waves, and interannual changes associated with ENSO. Although the present model is reasonably realistic, it nevertheless, like other models, underestimates a significant fraction of the actual variability present in the ocean. For instance, Fig. 16 compares zonal and meridional velocities of the model estimate and observations at 0°N, 140°W 150-m depth. Although interannual changes are reasonably simulated (especially in zonal velocity, albeit with a bias of approximately 20 cm s^{-1}), the model significantly underestimates the intraseasonal variability in meridional circulation. Given such limitation, the actual meridional transport of the interior pathway may be significantly larger in the ocean than what is estimated by the present model.

Such variability may help to better account for observed tracer distributions. Liu and Huang (1998) have suggested that the observed tritium maximum along the equator in the central Pacific (Fine et al. 1987) is due to the Mindanao Current transport leaving the western boundary before reaching the equator and joining the equator in the central Pacific. However, tritium concentration within the core of the Mindanao Current is smaller than the observed equatorial maximum, and the ridge of the tracer maximum in the thermocline leading to the equator occurs within the interior of the ocean. Temporal variability—in particular intraseasonal variability—may account for a significant fraction of the meridional, subtropical–tropical water exchange in the interior that contributes to the observed equatorial tritium maximum in the central Pacific. Nonaka and Takeuchi (2001) suggests that the larger sea surface tritium distribution in the eastern subtropics (i.e., inhomogeneous surface boundary condition) may also be important for the central Pacific tritium maximum. However, their modeling study includes temporal variability in the circulation as in this study and, therefore, its effect on the meridional exchange cannot be ruled out. Coles and Rienecker (2001) proposed seasonal variations in thermocline

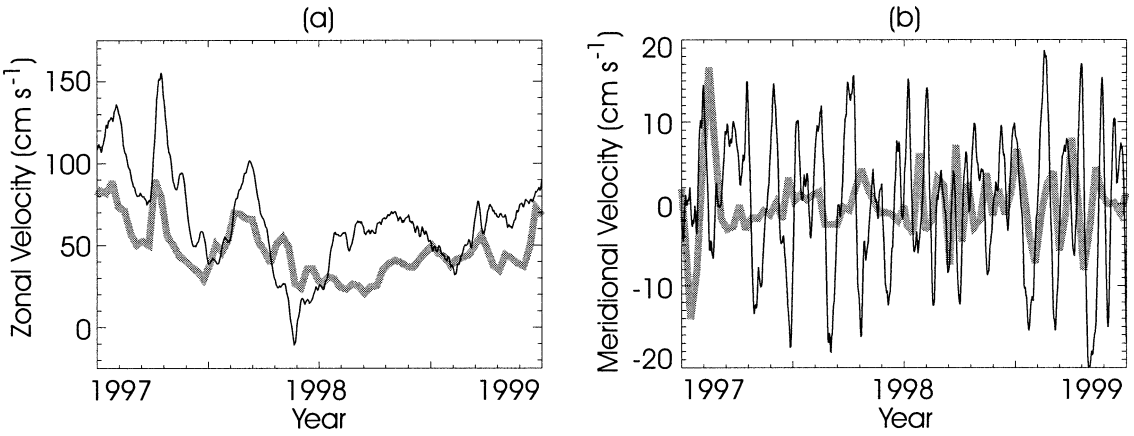

FIG. 16. Time series of (a) zonal and (b) meridional velocities at 0°N, 140°W, 150-m depth. Different curves are in situ measurements [Tropical Atmosphere–Ocean array (TAO)] (solid) and model estimate (gray).

thickness as a possible means of breaking the potential vorticity ''barrier,'' allowing a larger interior subtropical–tropical transport during autumn and early winter than otherwise inferred from a time-mean circulation. Results here, in particular, Figs. 13 and 15, suggest nonseasonal, intra-annual variability may contribute more to the exchange than do seasonal or interannual variations. The significance of stirring and mixing effects of the intra-annual variability may also help to account for the lack of coherence in observed temperature anomalies near the equator (e.g., Schneider et al. 1999).

d. Interannual to decadal variability

Differences between Figs. 5a and 5e illustrate interannual variability in the pathway of Niño-3 water. Interannual variability is further examined in Fig. 17 that shows, as a function of terminal instant, differences in 10-yr net meridional adjoint tracer transport of Niño-3 water along 5.7°S and 8.4°N. Individual values represent the amount of Niño-3 water that travels through different pathways during 10 years prior to reaching the Niño-3 region at indicated times on the abscissa. (Average values among the years are summarized in Table 1 as the average case.)

A general decadal weakening is found in the amount of Niño-3 water passing through low-latitude western boundary pathways in both hemispheres. An even larger weakening is evident in the interior pathway of the Northern Hemisphere, which may reflect the interdecadal slowing down of the meridional overturning circulation of the tropical Pacific Ocean (McPhaden and Zhang 2002).

The gradual change in the pathways is punctuated by large deviations associated with El Niño events, such as those in 1991–94 and in 1997. In the Northern Hemisphere, the Costa Rica Dome pathway virtually shuts down during El Niño, whereas the interior and LLWBC pathways strengthen. Similar increases are found in the Southern Hemisphere interior pathway, but not in the New Guinea Coastal Current and Undercurrent transport. The Southern Hemisphere LLWBC adjoint tracer transport is largest in 1992 but is smallest in 1997.

Differences in Niño-3 water origins between El Niño and non–El Niño years can be traced to the relaxation of the equatorial thermocline and the associated eastward, near-surface circulation during El Niño. Figures 18a and 18b show east–west sections of the adjoint tracer distribution along the equator at year −1 for Niño-3 waters of December 2000 and December 1997. For a non–El Niño year (Fig. 18a), Niño-3 water largely originates in the thermocline to the west, 1 year prior to the terminal instant, similar to averages seen in Fig. 7. In comparison, Niño-3 water for the peak of the 1997–98 El Niño event originates to the west but in the near-surface layer above the thermocline (Fig. 18b) reflecting El Niño's subsequent flattening of the thermocline (Fig. 19a) and eastward ''sloshing'' of water above the thermocline (Wyrtki 1975).

Differences are also evident in horizontal distribution of the adjoint tracer (Figs. 18c,d). Niño-3 water originates within the narrow equatorial zone 1 year prior in both El Niño and non–El Niño conditions. In non–El Niño years (Fig. 18c), the water is found largely in two separate patches; one toward the western end and the remaining water in Niño-3 to the east. In comparison, virtually all Niño-3 water of an El Niño year originates in the central equatorial Pacific. This central Pacific origin corresponds to the absence of the Costa Rica Dome pathway for Niño-3 water during El Niño (Fig. 17). Water in the central Pacific above the thermocline in Figs. 18b and 18d can be traced backward to thermocline water that originates in the LLWBC and interior pathways of the Northern and Southern Hemispheres.

It is also interesting to compare the edge of the adjoint tracer patch with the position of the isotherms. Picaut et al. (1996) show that the interannual movement of the eastern edge of the western equatorial Pacific warm pool is largely controlled by zonal advection associated with

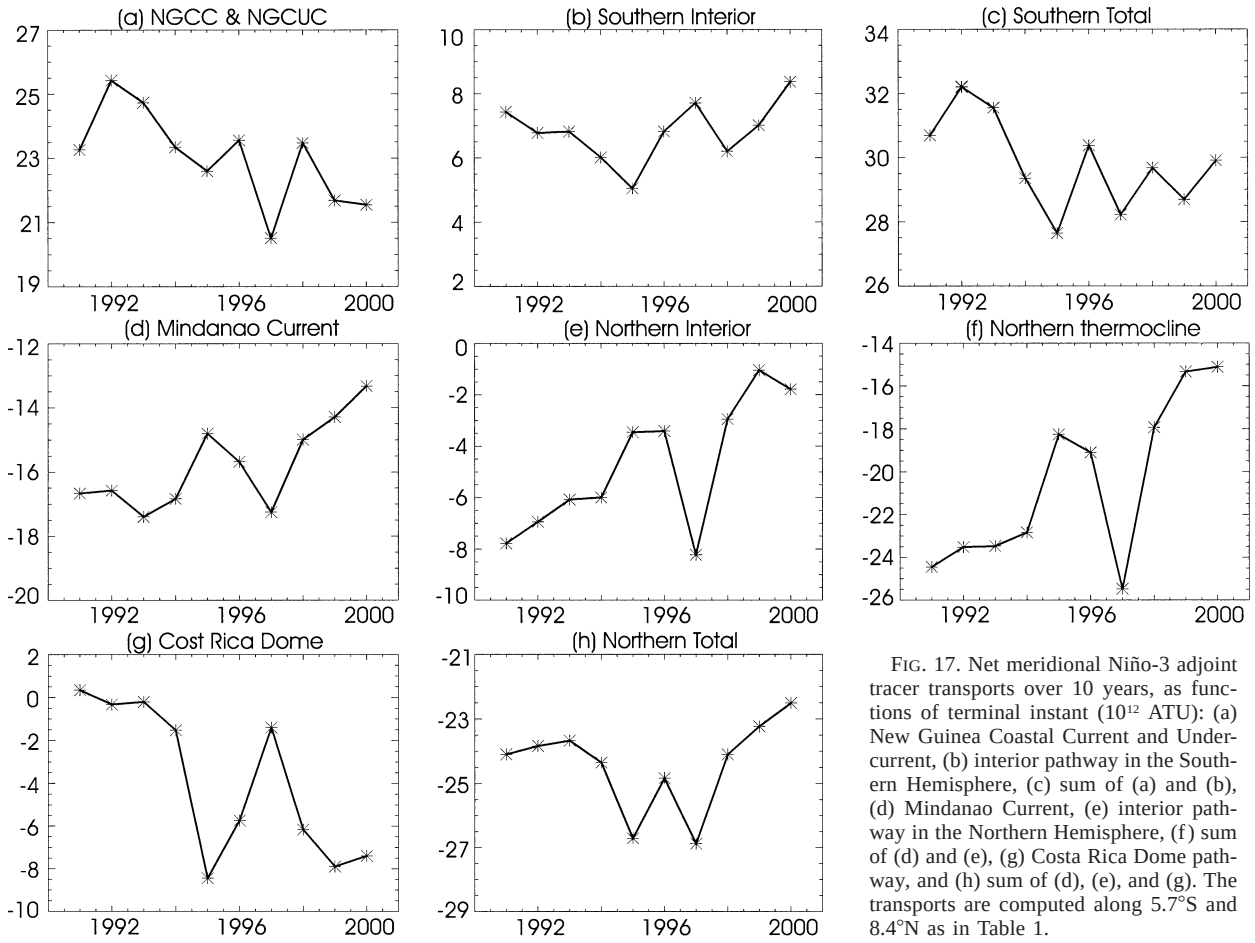

FIG. 17. Net meridional Niño-3 adjoint tracer transports over 10 years, as functions of terminal instant (10^{12} ATU): (a) New Guinea Coastal Current and Undercurrent, (b) interior pathway in the Southern Hemisphere, (c) sum of (a) and (b), (d) Mindanao Current, (e) interior pathway in the Northern Hemisphere, (f) sum of (d) and (e), (g) Costa Rica Dome pathway, and (h) sum of (d), (e), and (g). The transports are computed along 5.7°S and 8.4°N as in Table 1.

El Niño–La Niña. Figure 19 shows isotherms at the end of 1997. Consistent with observations of the zonal migration of the warm pool, a comparison of Figs. 18 and 19 shows that the movement of the western end of the Niño-3 adjoint tracer patch largely coincides with the 28°C isotherm (thick contour). In contrast, because of mixing, isotherms in the center and eastern end of the adjoint tracer patch do not coincide with particular isotherms.

e. Where does Niño-3 water go?

In the previous sections, we have focused on analyzing from where Niño-3 water comes. For completeness, we will now examine where Niño-3 water goes by integrating a passive tracer forward in time (as opposed to the backward adjoint tracer integrations discussed previously.) As in the adjoint tracer integration, a mean climatological pathway of the Niño-3 water circulation is estimated by averaging passive tracer distributions of different experiments. These experiments consist of 10 forward, 10-yr-long, tracer integrations, each starting from the end of a different year, from 1981 to 1990. Each experiment is initialized by a unit passive tracer concentration (ATU m^{-3}) in the surface layer (10 m thick) of Niño-3 and zero elsewhere. The average pathway and destination of Niño-3 water are illustrated by average, depth-integrated tracer distributions and vertical cross sections in Figs. 20 and 21.

Niño-3 water is advected westward by the South Equatorial Current and is split meridionally by Ekman transport away from the equator (Fig. 20). As a result, the cloud of Niño-3 water off the equator has a characteristic southwest-to-northeast tilt in the Northern Hemisphere and a northwest-to-southeast tilt in the Southern Hemisphere (Fig. 20a). These clouds of Niño-3 tracer flow poleward in each hemisphere in the central Pacific into the equatorward half of the subtropical gyres, converging toward latitudes where meridional Ekman flux is zero (thick dashed contour in Fig. 20). Water at the western end of these clouds reaches the western boundary where parts of the water feed the subtropical, western boundary currents (Kuroshio and East Australian Current) that advect the Niño-3 water into the poleward half of the subtropical gyres (Fig. 20b). Part of this water also makes its way into the Indian Ocean through the Indonesian passages (Figs. 20b,c). Some of this water is also recirculated toward

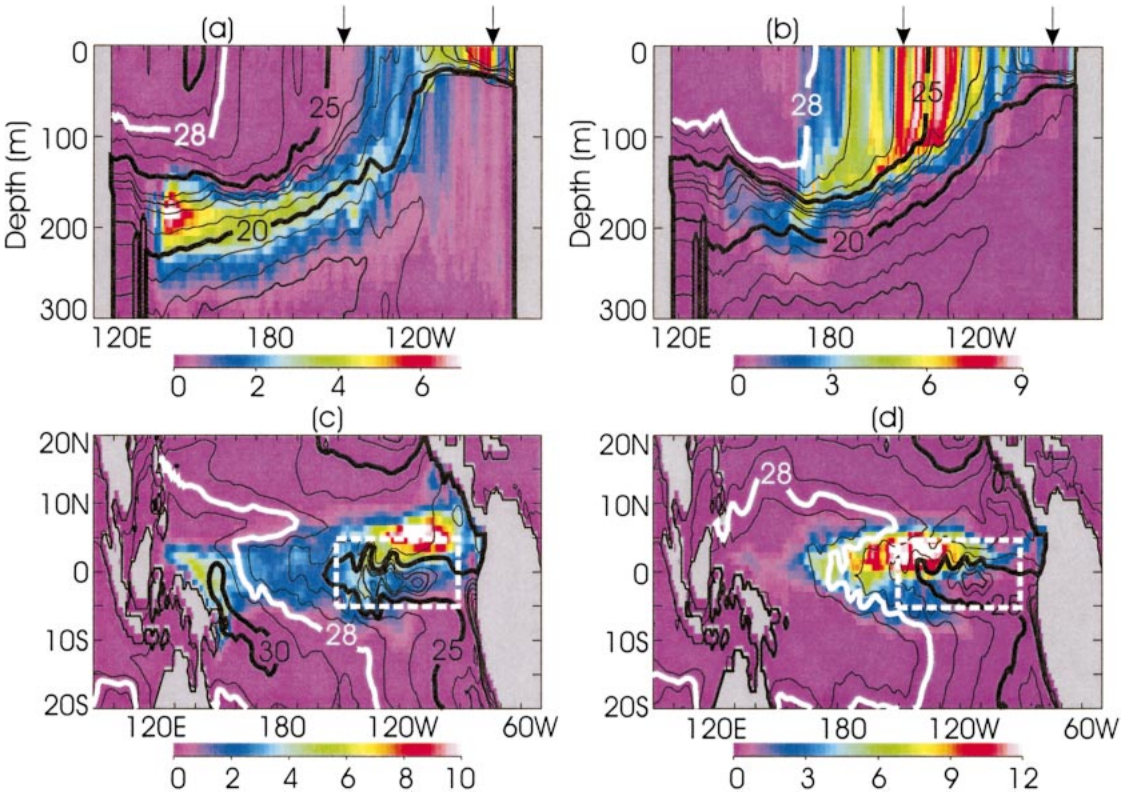

FIG. 18. Distribution of adjoint tracer at year −1 for Niño-3 water of (a), (c) Dec 2000 and (b), (d) December 1997. Panels (a) and (b) are vertical cross sections along equator, whereas (c) and (d) are depth integrations of the adjoint tracer. Arrows in (a) and (b) and the white dashed boxes in (c) and (d) denote the extent of Niño-3. Units are 10^{-2} ATU m^{-3} and ATU m^{-2}, respectively. Contours are isotherms along the equator and at the sea surface, with contour intervals of 1°C. The thick white contour is the 28°C isotherm that largely coincides with the western end of the Niño-3 water during ENSO. See text for discussion.

the equator by the LLWBCs, but the zonal extent of this water mass along the equator is limited and gradually recedes to the west as the water is increasingly expelled into the subtropics and Indian Ocean (Figs. 20b,c). After 10 years, 46% of the original Niño-3 water is found in the North Pacific, 38% is in the South Pacific, and the remaining 16% flows into the Indian Ocean.

The horizontal circulation of Niño-3 water occurs near the surface mainly above the thermocline (Fig. 21). At year 6, some water is seen to have subducted into the upper thermocline about 20°S and 20°N in the western basin (Fig. 21b), as evidenced by the subsurface maxima in forward tracer concentration. Farther poleward, about 30° from the equator, Niño-3 water advected by the subtropical western boundary currents begins to penetrate the lower thermocline in both hemispheres.

The destination of Niño-3 water is in stark contrast with the origin of Niño-3 water discussed in section 5a (Figs. 6 and 7). Niño-3 water was found to originate in the eastern half of the subtropical gyre (Fig. 6f), flowing equatorward within the thermocline (Fig. 7). In contrast, after reaching Niño-3, this water mass flows poleward, remaining above the thermocline, and returns to the subtropics (Fig. 21b) but in the western half of the semi-closed, subtropical gyres (Fig. 20). This suggests that the subtropical cell is not a closed circulation that might be inferred from the zonally integrated meridional stream function shown in Fig. 2.

6. Summary and conclusions

The nature of subtropical–tropical water mass exchange is investigated using evolutions of a passive tracer and its adjoint based on circulation estimates of an ocean general circulation model. In the absence of sources and sinks, the evolution of passive tracers with time can be understood as describing where the water mass initially tagged by the tracer goes. In comparison, the evolution of adjoint passive tracers backward in time can be identified as describing from where the tagged water mass at the terminal instant comes. The contents of tracer and adjoint tracer at a particular location, relative to their initial and terminal values of the tagged water mass, respectively, quantify the fraction of the original water contained in the subject volume. The movement of the tracers through the fluid domain identifies the pathway of the tagged water mass.

The tracers reflect effects of both advection and

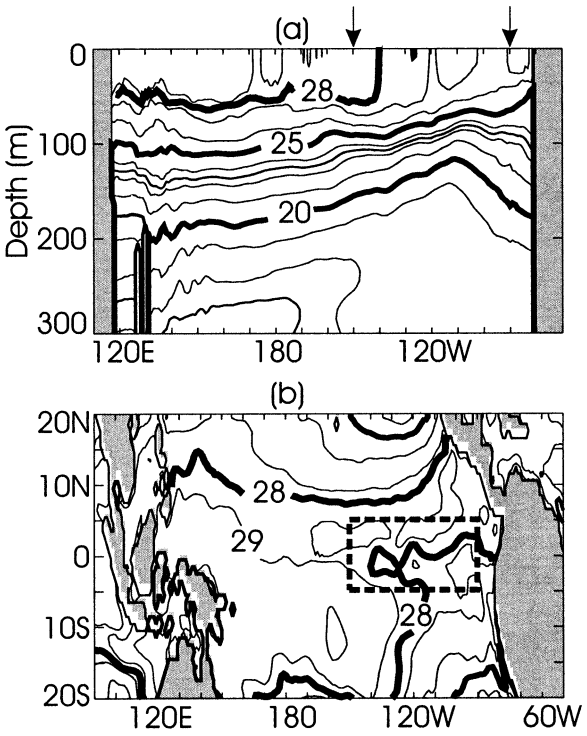

FIG. 19. (a) Zonal section of temperature along the equator and (b) sea surface temperature in Dec 1997. Arrows in (a) and dashed box in (b) denote extent of Niño-3. Contours are as in Fig. 18.

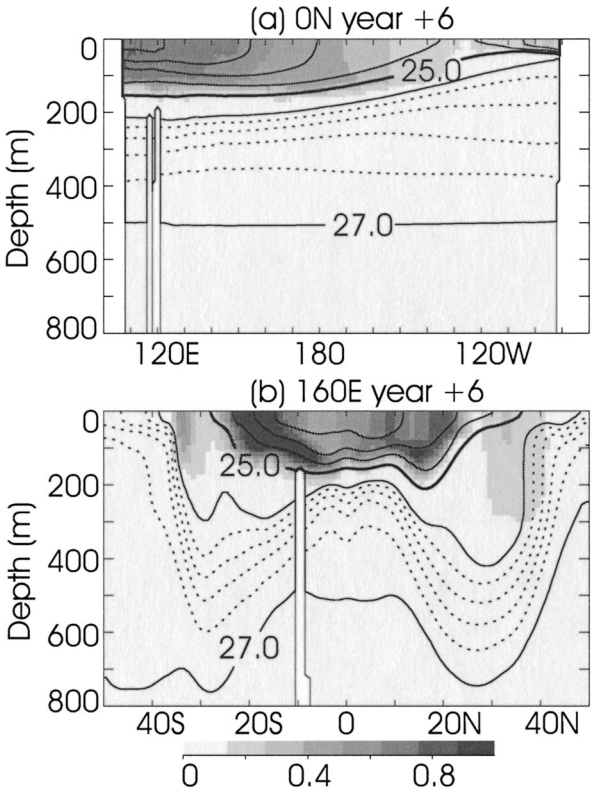

FIG. 21. Average vertical sections of Niño-3 passive tracer at year 6: (a) 0°N and (b) 160°E. Units are in 10^{-2} ATU m^{-3}. Contours are potential density as in Fig. 7.

mixing and account for temporal variability in the circulation, thus providing a powerful means to quantify the origin, pathway, and destination of water masses. Divergence, mixing, and time variability in the circulation make inferences of water mass pathways difficult from maps of Eulerian velocity. Lagrangian particles and float trajectories are chaotic, in the sense that slight perturbations can lead to widely different trajectories, resulting in typical ''spaghetti'' diagrams that are difficult to interpret. (The chaotic nature of trajectories reflect straining by shear in the circulation. No finite parcel of water remains coherent but is strained and stirred together with its surroundings.) In the absence of mixing, the evolution of passive tracers and their adjoints is equivalent to averaging pathways of an infinite number of particle trajectories

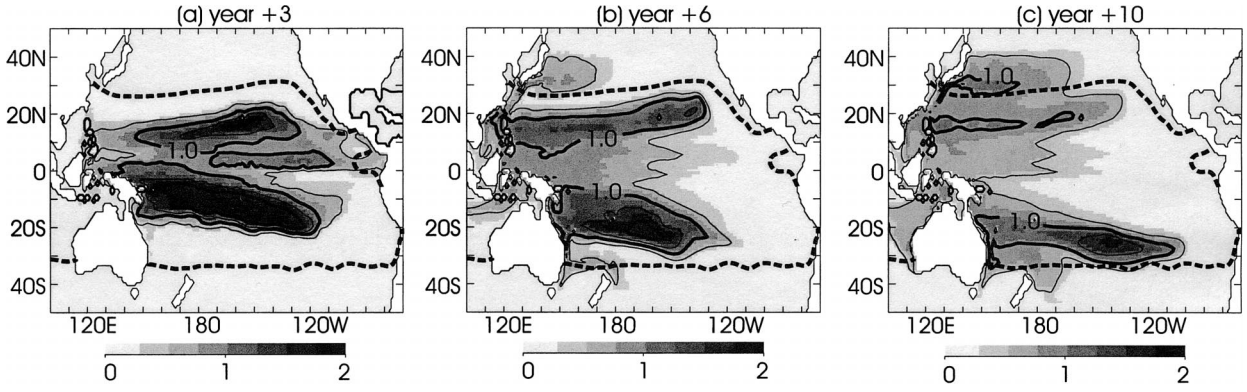

FIG. 20. Average horizontal distribution of Niño-3 tracer as a function of years from initial time; (a) year 3, (b) year 6, and (c) year 10. The values are vertically integrated passive tracer (ATU m^{-2}) averaged among 10 experiments, each initialized from the end of a different year between 1981 to 1990. The distribution at the initial time (year 0) is uniformly 10 (ATU m^{-2}) within Niño-3 and zero elsewhere. Contour intervals are 0.5 ATU m^{-2}, and values for 1.0, 2.0, and 3.0 ATU m^{-2} are shown in thick contours. The thick dashed curve indicates the zero time-averaged zonal wind stress.

forward and backward in time, respectively, averaging the multiple pathways that water of finite volume can take from one point to another. Distribution of tracers, unlike individual particle trajectories, stay coherent, and the mean pathways can be readily deduced from their evolution. Moreover, although tracers can account for effects of mixing, in general, particle trajectories cannot.

Holzer and Hall (2000) used a tracer and its adjoint in studying transit times between a source and a target (age spectrum) in fluid circulation. Vukićević and Hess (2000) employed an adjoint passive tracer to investigate the source of chemical species in the atmosphere. The present study is the first study of which we are aware to employ an adjoint passive tracer in deducing the origin and pathway of water masses in the ocean. Marotzke et al. (1999) examined the sensitivity of meridional heat transport in the Atlantic Ocean to various model controls, in particular, to temperature and salinity perturbations using the model's adjoint. While the individual sensitivity to temperature and to salinity also illustrates aspects of the water mass circulation, the dynamic effects of temperature and salinity result in sensitivities related to planetary waves that are difficult to separate from circulation pathways. Marotzke et al. (1999) illustrate how temperature and salinity sensitivities can be combined in a density-compensating manner to isolate the kinematic sensitivity of the circulation, similar to the physical interpretation of the adjoint passive tracer. However, nonlinearities of the equation of state can make it difficult to eliminate dynamic effects by a simple linear combination. Moreover, their dynamic effects render calculation of the temperature and salinity sensitivities more computationally demanding than that of the passive tracer (cf. the appendix.)

This study focuses on the pathway of the water mass that occupies the surface layer of the Niño-3 region, the area in the eastern equatorial Pacific Ocean between 5°S and 5°N and between 150° and 90°W. This water mass is of particular interest because sea surface temperature in this region provides a key index for ENSO. In particular, Gu and Philander (1997) postulate that thermal anomalies advected to the equator by subtropical–tropical water mass exchange underlie the observed interdecadal variability in the nature of ENSO.

The adjoint tracer evolution demonstrates that Niño-3 water largely comes from the thermocline by upwelling and mixing. This water in the equatorial thermocline arrives at the equator from the subtropics via distinct circuitous routes. Water is subducted into the thermocline in the eastern subtropical gyre near regions where the $\sigma_\theta = 25$ kg m^{-3} isopycnal outcrops in winter. The subducted water is subsequently advected equatorward and westward within the thermocline. Approximately 80% of this subducted water mass flows through the low-latitude western boundary currents (LLWBCs) in their respective hemispheres before reaching the equator. The remaining 20% flows through the interior ocean directly toward the equator. After reaching the equator, the water is quickly advected to the east by the Equatorial Undercurrent. The representative transit time from the subtropics to the equator is approximately 10 years, but once at the equator the water that reaches Niño-3 rapidly converges eastward within 1 year.

The model also reveals that part of the Niño-3 water (5% of the total) originates from the midlatitude coastal regions off North America and flows equatorward along the eastern boundary of the North Pacific Ocean. This eastern boundary pathway is confined to depths near the surface and is connected to the Niño-3 region via the Costa Rica Dome. The existence of such a coastal pathway is also supported by hydrographic observations (Kessler 2002).

The amount of Niño-3 water originating from the Southern Hemisphere is larger than that from the Northern Hemisphere. Over 10 years, on average, 27% and 39% of the Niño-3 water mass can be traced back to thermocline waters of the Northern and Southern Hemispheres, respectively. The remainder consists of surface, Northern Hemisphere, coastal waters along North America (5%), and recirculated tropical water masses (29%).

The strength of the pathways has considerable interannual to decadal variabilities. In particular, the thermocline pathway in both hemispheres appears to be slowing down during the last decade, consonant with recent inferences from observed changes in wind stress (McPhaden and Zhang 2002). Differences are also evidenced that illustrate distinct origins of the Niño-3 water mass for El Niño and non–El Niño periods. In particular, the adjoint tracer reveals the eastward ''sloshing'' of near-surface water due to the relaxation of the thermocline associated with El Niño (Wyrtki 1975). A larger portion of Niño-3 water originates from the subtropical thermocline, especially from the Northern Hemisphere during El Niño events. In comparison, there is little contribution of Northern Hemisphere coastal waters during El Niño.

A particularly noteworthy finding of this study is the effect of intra-annual variability of the circulation on the mean pathway of the water mass (Fig. 13). Pathway estimates using time-mean or temporally filtered circulations result in a much smaller interior pathway and in a negligible North American coastal pathway, relative to the LLWBC pathways. Stirring effects of temporally varying circulation, combined with the large meridional shear in zonal tropical circulation, short circuits the pathway of water masses, allowing a much larger interior meridional exchange than otherwise. Pathway estimates based on time-mean circulation may significantly underestimate the relative magnitude of the interior, subtropical–tropical water mass exchange. Moreover, observed intra-annual variability in velocity is much larger than the variability of most numerical sim-

ulations, including the variability of the present model. Consequently the magnitude of the interior pathways estimated herein likely underestimates actual values. The large intra-annual variability in meridional velocity observed in the Tropics, and its effect on meridional water mass exchange, may account for the observed tritium maximum in the central equatorial Pacific. Indeed, heat transport associated with eddy variability is estimated to be a dominant element in the meridional upper-ocean heat transport (Wang and McPhaden 2001). A similar balance is plausible for water mass and tracer transport.

The destination of Niño-3 water over 10 years revealed by forward integrations of a passive tracer consists of subtropical gyres of the North (46%) and South (38%) Pacific Oceans and flows into the Indian Ocean (16%). The circulation is confined largely to the surface in contrast with the 10+-year-long pathway deduced by the adjoint tracer. Moreover, while Niño-3 water originates in the eastern half of the subtropical gyre, the destination of Niño-3 water is confined to the western half of the subtropical basin where water recirculates within the subtropical gyre. The subtropical cell that describes the net, time-mean, advective pathway of subtropical–tropical water exchange does not consist of a closed circuit, as might be inferred from a zonally integrated meridional overturning streamfunction.

The adjoint tracer has considerably more potential in providing new information about the ocean than the particular application described in this study. Adjoint tracers can be utilized to investigate, for instance, the origins of various mode waters and different chemical species, a subject central to understanding the general circulation of the ocean. Budgets of heat, salt, and other chemical elements following the simulated passive tracer can provide insight into transformation mechanisms of the tracer-tagged water mass. These and other applications will be pursued in future studies.

Acknowledgments. This study is a contribution of the Consortium for Estimating the Circulation and Climate of the Ocean (ECCO) funded by the National Oceanographic Partnership Program. Support was also provided by the TOPEX/Poseidon and the *Jason-1* Projects. This research was carried out in part at the Jet Propulsion Laboratory (JPL), California Institute of Technology, under contract with the National Aeronautics and Space Administration. Computational support of the JPL Supercomputing Project is gratefully acknowledged.

APPENDIX

Model Implementation of Tracer and Its Adjoint

Passive tracer time stepping in the model is implemented in the same way as the time stepping of temperature and salinity, as per (2), except for external boundary conditions. Unlike temperature and salinity, the tracer being passive does not affect density, the velocity field, and the mixing rates. Consequently, passive tracer integrations, in contrast to those for temperature and salinity, can be conducted independent of evaluating the velocity field and mixing coefficients. In particular, (2) can be integrated using precomputed velocities ($\mathbf{u}$) and mixing tensors (κ) that are saved periodically for analyses. Such ''offline'' integration avoids having to reevaluate the time-evolving model state at each individual model time step. Additionally, larger time steps (2 h for the present model configuration) can be taken in the numerical integration of the tracer, as compared with that required for computational stability of the velocity field (1 h). Similar offline tracer models were used by Follows et al. (1996).

Figures 4a and 4b and the analyses in section 5e were conducted using such offline tracer integrations, which used velocities and mixing tensors that had been saved every 10 days (10-day running averages). However, such offline integrations could incur inaccuracies due to effects of high-frequency changes in the circulation, not resolved by the precomputed sampling of $\mathbf{u}$ and κ. Figures A1a and A1b show the same forward tracer integration as in Figs. 4a and 4b but integrating the tracer equation simultaneously with the model circulation. Differences between these two results are negligible and the 10-day sampling appears to be sufficient in resolving the essential features of the water mass circulation.

In continuous form, the adjoint tracer equation is

$$-\frac{\partial c}{\partial t} = \mathbf{u} \cdot \nabla c + \nabla \cdot \kappa \nabla c. \qquad \text{(A1)}$$

Given $\mathbf{u}$ and κ, integrating (A1) backward in time is theoretically identical with integrating (2) forward in time, except for the sign of the advective term. Therefore, evolution of the adjoint tracer can be evaluated backward in time using the same numerical program as the ''offline'' forward tracer integration but reversing the sign of advection (''approximate adjoint''). Although equivalent in the continuous limit, the numerical procedure of such approximation [finite-difference approximation of (A1)]. is not identical to that of the adjoint of the finite-difference equation [(8); e.g., Sirkes and Tziperman 1997]. However, such differences are minor, as shown in Figs. A1c and A1d. These are equivalent to Figs. 4c and 4d, but are computed employing such an approximate adjoint. The advantage of such approximation is its simplicity and its computational efficiency. The formal adjoint of the offline tracer model [(8)] involves several additional steps needed to evaluate and to store supplementary variables that are different from the approximate adjoint.

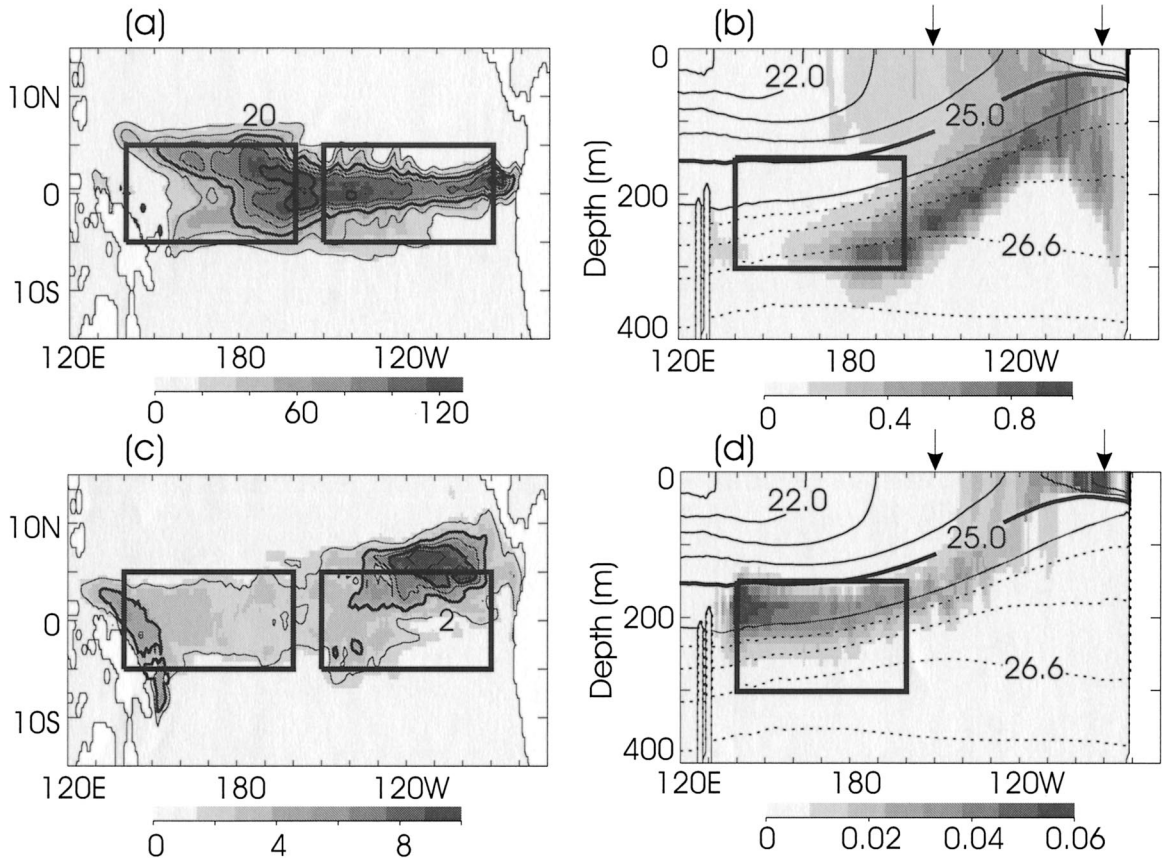

FIG. A1. Tracer and adjoint tracer distribution similar to Fig. 4, except for (a), (b) the online integration of the passive tracer and (c), (d) the utilization of the approximate adjoint. See the caption of Fig. 4 for a description of the variables and the text for further discussion.

REFERENCES

Barnier, B., L. Siefridt, and P. Marchesiello, 1995: Thermal forcing for a global ocean circulation model using a three-year climatology of ECMWF analyses. *J. Mar. Syst.*, **6,** 363–380.

Butt, J., and E. Lindstrom, 1994: Currents off the east coast of New Ireland, Papua New Guinea, and their relevance to regional undercurrents in the western equatorial Pacific Ocean. *J. Geophys. Res.*, **99,** 12 503–12 514.

Coles, V. J., and M. M. Rienecker, 2001: North Pacific subtropical–tropical gyre exchanges in the thermocline: Simulations with two isopycnic OGCMs. *J. Phys. Oceanogr.*, **31,** 2590–2611.

da Silva, A. M., C. C. Young, and S. Levitus, 1994: *Algorthims and Procedures.* Vol. 1, *Atlas of Surface Marine Data 1994,* NOAA Atlas NESDIS 6, U.S. Department of Commerce, 83 pp.

Deser, C., M. A. Alexander, and M. S. Timlin, 1996: Upper-ocean thermal variations in the North Pacific during 1970–1991. *J. Climate,* **9,** 1840–1855.

Fiedler, P. C., 2002: The annual cycle and biological effects of the Costa Rica Dome. *Deep-Sea Res.*, **49,** 321–338.

Fine, R. A., J. L. Reid, and H. G. Ostlund, 1981: Circulation of tritium in the Pacific Ocean. *J. Phys. Oceanogr.*, **11,** 3–14.

——, W. H. Peterson, and H. G. Ostlund, 1987: The penetration of tritium into the tropical Pacific. *J. Phys. Oceanogr.*, **17,** 553–564.

Follows, M. J., R. G. Williams, and J. C. Marshall, 1996: The solubility pump of carbon in the subtropical gyre of the North Atlantic. *J. Mar. Res.*, **54,** 605–630.

Gent, P. R., and J. C. McWilliams, 1990: Isopycnal mixing in ocean circulation models. *J. Phys. Oceanogr.*, **20,** 150–155.

Gu, D. F., and S. G. H. Philander, 1997: Interdecadal climate fluctuations that depend on exchanges between the Tropics and extratropics. *Science,* **275,** 805–807.

Holzer, M., and T. M. Hall, 2000: Transit-time and tracer-age distributions in geophysical flows. *J. Atmos. Sci.*, **57,** 3539–3558.

Huang, B., and Z. Liu, 1999: Pacific subtropical–tropical thermocline water exchange in the National Centers for Environmental Prediction ocean model. *J. Geophys. Res.*, **104,** 11 065–11 076.

Huang, R. X., and Q. Wang, 2001: Interior communication from the subtropical to the tropical oceans. *J. Phys. Oceanogr.*, **31,** 3538–3550.

Ji, M., A. Leetmaa, and V. E. Kousky, 1996: Coupled model predictions of ENSO during the 1980s and the 1990s at the National Centers for Environmental Prediction. *J. Climate,* **9,** 3105–3120.

Johnson, G. C., and M. J. McPhaden, 1999: Interior pycnocline flow from the subtropical to the equatorial Pacific Ocean. *J. Phys. Oceanogr.*, **29,** 3073–3089.

Kalnay, E., and Coauthors, 1996: The NCEP/NCAR 40-Year Reanalysis Project. *Bull. Amer. Meteor. Soc.*, **77,** 437–471.

Kessler, W. S., 2002: Mean three-dimensional circulation in the northeast tropical Pacific. *J. Phys. Oceanogr.*, **32,** 2457–2471.

Large, W. G., J. C. McWilliams, and S. C. Doney, 1994: Oceanic vertical mixing: A review and a model with a nonlocal boundary-layer parameterization. *Rev. Geophys.*, **32,** 363–403.

——, G. Danabasoglu, S. C. Doney, and J. C. McWilliams, 1997: Sensitivity to surface forcing and boundary layer mixing in a global ocean model: Annual mean climatology. *J. Phys. Oceanogr.*, **27,** 2418–2447.

Lee, T., I. Fukumori, D. Menemenlis, Z. Xing, and L.-L. Fu, 2002:

Effects of the Indonesian Throughflow on the Pacific and Indian Oceans. *J. Phys. Oceanogr.,* **32,** 1404–1429.

Levitus, S., 1982: *Climatological Atlas of the World Ocean.* NOAA Prof. Paper 13, 173 pp. and microfiche.

——, and Coauthors, 1998: *Introduction.* Vol. 1, *World Ocean Database 1998,* NOAA Atlas NESDIS 18, 346 pp.

Liu, Z., 1994: A simple model of the mass exchange between the subtropical and tropical ocean. *J. Phys. Oceanogr.,* **24,** 1153–1165.

——, and B. Huang, 1998: Why is there a tritium maximum in the central equatorial Pacific thermocline? *J. Phys. Oceanogr.,* **28,** 1527–1533.

——, S. G. H. Philander, and R. C. Pacanowski, 1994: A GCM study of tropical–subtropical upper-ocean water exchange. *J. Phys. Oceanogr.,* **24,** 2606–2623.

Lu, P., and J. P. McCreary, 1995: Influence of the ITCZ on the flow of thermocline water from the subtropical to the equatorial Pacific Ocean. *J. Phys. Oceanogr.,* **25,** 3076–3088.

——, ——, and B. A. Klinger, 1998: Meridional circulation cells and the source waters of the Pacific Equatorial Undercurrent. *J. Phys. Oceanogr.,* **28,** 62–84.

Marotzke, J., R. Giering, K. Q. Zhang, D. Stammer, C. Hill, and T. Lee, 1999: Construction of the adjoint MIT ocean general circulation model and application to Atlantic heat transport sensitivity. *J. Geophys. Res.,* **104,** 29 529–29 547.

Marshall, J. C., A. Adcroft, C. Hill, L. Perelman, and C. Heisey, 1997: A finite-volume, incompressible Navier–Stokes model for studies of the ocean on parallel computers. *J. Geophys. Res.,* **102,** 5753–5766.

McCreary, J. P., and P. Lu, 1994: Interaction between the subtropical and equatorial ocean circulations: The subtropical cell. *J. Phys. Oceanogr.,* **24,** 466–497.

McPhaden, M. J., and R. A. Fine, 1988: A dynamical interpretation of the tritium maximum in the central equatorial Pacific. *J. Phys. Oceanogr.,* **18,** 1454–1457.

——, and D. Zhang, 2002: Slowdown of the meridional overturning circulation in the upper Pacific Ocean. *Nature,* **415,** 603–608.

Nonaka, M., and K. Takeuchi, 2001: Tropical subsurface salinity and tritium distributions in the Pacific: Their differences and formation mechanisms. *J. Phys. Oceanogr.,* **31,** 1388–1395.

——, S.-P. Xie, and J. P. McCreary, 2002: Decadal variations in the subtropical cells and equatorial Pacific SST. *Geophys. Res. Lett.,* **29,** 1116, doi:10.1029/2001GL013717.

Picaut, J., M. Ioualalen, C. Menkes, T. Delcroix, and M. J. McPhaden, 1996: Mechanism of the zonal displacements of the Pacific warm pool: Implications for ENSO. *Science,* **274,** 1486–1489.

Qiu, B., 1999: Seasonal eddy field modulation of the North Pacific subtropical countercurrent: TOPEX/Poseidon observations and theory. *J. Phys. Oceanogr.,* **29,** 2471–2486.

Redi, M., 1982: Oceanic isopycnal mixing by coordinate rotation. *J. Phys. Oceanogr.,* **12,** 1154–1158.

Reynolds, R. W., and T. M. Smith, 1994: Improved global sea surface temperature analyses using optimum interpolation. *J. Climate,* **7,** 929–948.

Rothstein, L. M., R.-H. Zhang, A. J. Busalacchi, and D. Chen, 1998: A numerical simulation of the mean water pathways in the subtropical and tropical Pacific Ocean. *J. Phys. Oceanogr.,* **28,** 322–343.

Schneider, N., A. J. Miller, M. A. Alexander, and C. Deser, 1999: Subduction of decadal North Pacific temperature anomalies: Observations and dynamics. *J. Phys. Oceanogr.,* **29,** 1056–1070.

Sirkes, Z., and E. Tziperman, 1997: Finite difference of adjoint or adjoint of finite difference? *Mon. Wea. Rev.,* **125,** 3373–3378.

Talley, L. D., 1988: Potential vorticity distribution in the North Pacific. *J. Phys. Oceanogr.,* **18,** 89–106.

Vukicevic, T., and P. Hess, 2000: Analysis of tropospheric transport in the Pacific Basin using the adjoint technique. *J. Geophys. Res.,* **105,** 7213–7230.

Wang, W. M., and M. J. McPhaden, 2001: Surface layer temperature balance in the equatorial Pacific during the 1997–98 El Niño and 1998–99 La Niña. *J. Climate,* **14,** 3393–3407.

Wyrtki, K., 1975: El Niño—The dynamic response of the equatorial Pacific Ocean to atmospheric forcing. *J. Phys. Oceanogr.,* **5,** 572–584.

Zhang, R.-H., L. M. Rothstein, and A. J. Busalacchi, 1998: Origin of upper-ocean warming and El Niño change on decadal scales in the tropical Pacific Ocean. *Nature,* **391,** 879–883.